ANNALS OF GEOPHYSICS, 66, 3-4, SE318; 2023; doi:10.4401/ag-8889
OPEN ACCESS

Development of Synthetic Ground Motion-based Attenuation Relationship for Bihar Region Considering Central Seismic Gap for Seismic Ground Response Analysis

Prabhakar Kumar[1], Shiv Shankar Kumar[*,1] and
Harinarayan Nelliparanbil Hareeshkumar[2]

(1) Department of Civil Engineering, National Institute of Technology (NIT) Patna-800005
(2) Department of Civil Engineering, Universal Engineering College Thrissur, Kerala

Article history: received August 4, 2022; accepted May 10, 2023

Abstract

Ground Motion Prediction Equation (GMPE) is one of the significantly important tools to perform the seismic hazards analysis of any region. Therefore, the development of GMPEs at the bedrock level is utmost important especially when the region does not have any earthquake recording stations. The present study discussed the development of a GMPE at bedrock level for the Bihar region based on the stochastic model. The different seismic parameters such as magnitudes (M_w) 4.0-8.5, spectral periods of 0-10 s and distances up to 300 km have been considered for the stochastic model. Based on the results, it was found that the stochastic model is capable to predict the ground motion synthetically and the proposed GMPE, for Bihar region, predicts the spectral acceleration in most precise way. Further, the ground motion amplification analysis was carried out using synthetically generated bedrock motion to analyze the effect of soil deposits on the amplification or de-amplification of the bedrock peak ground acceleration. It was found that that the seismic wave gets amplified at ground level by 10% to 70% from the input motion PGA ranging from 0.175g-0.435g, indicating amplification and de-amplification of seismic wave. The maximum spectral acceleration at surface level was also found to be increased by approximately 60%, 56% and 27%, when bedrock input motion of PGA = 0.175g, 0.256g and 0.435g, respectively. Thus, based on the results, it can be stated that the developed GMPE can be used to assess the seismic hazards analysis in Bihar region. Further, it can be suggested that there is a need of the development of a predictive attenuation relationship at the surface level PGA, for Bihar region or any earthquake prone area, incorporating different site classes and regional seismicity since, the seismic wave amplified due to the presence of soil deposits.

Keywords: GMPE; Central seismic gap; Bihar region; Spectral acceleration; Site amplification

1. Introduction

Earthquake is one of the most devastating natural hazards, which severely impact the human life as well as the economy of the country. The earthquake (EQ) devastation can be of several modes such as ground shaking, ground rupture, landslides, tsunamis, liquefaction, subsidence, and fire. Therefore, it can be stated that the EQ is one of the natural hazards, which may turn into multi-hazards. Among the aforementioned impacts of the EQ, ground shaking has the most severe influence on the stability of structures [Bird and Bommer, 2004]. Though the stability of the structure is influenced by several parameters along with the ground shaking such as source, site conditions, and regional seismicity, the region-specific seismic hazard analysis is one of the significantly important ways to assess the appropriate ground shaking parameters such as acceleration, velocity, or displacement [Harinarayan and Kumar 2020a]. The variations of these parameters, at ground level, depend on the soil conditions above the bedrock level. The sub-surface geology and the depth of soil up to 30 m have a significant impact on the amplification and de-amplification of the seismic wave [Kumar et al., 2018b]. The region-specific GMPEs are limited in India which hinders the precise seismic hazard assessment [National Disaster Management Authority (NDMA), 2010; Anbazhagan et al., 2013a]. Seismic waves of past Himalayan earthquakes (EQs) often reach the north Indian cities through the propagation medium, unlike rock sites. Thus, to develop a precise regional GMPE relationship applicable to the Indian plains, consideration of the regional geological characteristics of eastern India is the need of the hour [Harinarayan and Kumar, 2020b]. Most of the GMPEs developed in India were for the north-eastern region [Nath et al., 2005, 2009; Baruah et al., 2009; Gupta, 2010] or northern region [Singh et al., 1996; Sharma, 1998; Sharma and Bungum, 2006; Ramkrishnan et al., 2019; Harinarayan and Kumar, 2020b]. Therefore, an attempt is hereby made to develop a GMPE for the Bihar region due to inherent seismicity from foothills of Bihar-Nepal Himalaya, considering local site features.

The Himalayan region has experienced severe EQs of magnitudes greater than 6.0 in the past and recent past: 1803 Uttarkashi EQ, 1833 Bihar EQ, 1897 Assam EQ, 1905 Kangra EQ, 1934 Bihar-Nepal EQ, 1950 Assam EQ, 1988 Bihar-Nepal EQ, 1999 Chamoli EQ, 2005 Kashmir EQ, 2011 Sikkim EQ and 2015 Nepal EQ. The continuous subduction of the Indian plate towards the Eurasian plate is a major reason for the occurrence of these EQs in the Himalayan region. Several faults and lineaments associated with the convergence of the Indian and Eurasian plates cause crustal deformation in the entire Himalayan region which makes the region one of the most seismically active regions worldwide. Despite being active, the Himalayan region contains various seismic gaps which are the segment of the active fault which has not produced any significant EQs for a longer duration. The entire Himalayan region has been divided into three segments of the seismic gap: Assam seismic gap, Central Seismic gap and Kashmir seismic gap shown in Figure 1 [Khattri, 1987 and 1999]. The seismic gap segment between the 1934 Nepal-Bihar EQ and the 1950 Assam EQ is called the "Assam seismic gap" and, the large EQ that occurred in this region was the 1897 Shillong EQ. The seismic gap between the 1905 Kangra EQ and the 1934 Nepal-Bihar EQ is called the "Central seismic gap". This seismic gap was the witness of two major EQs i.e., 1803 and 1833 EQs of M_w 7.8, which is lesser than the magnitude (M_w) of 8.5 reported by Khattri [1999]. Khattri [1999] has reported that the probability of occurrence of an EQ of $M_w > 8.0$, in near future, is 0.52; mainly due to the accumulation of strain energy in the unbroken segment of the central seismic gap for a longer duration. Further, the seismic gap between the 1905 Kangra EQ and the 2005 Kashmir EQ is called the "Kashmir seismic gap". Although the pre-prediction of an EQ is quite difficult, the probability of occurrence of an EQ in the future can be done based on the past seismic event and their tectonic features in the related seismic gap. A recent 2015 Nepal EQ of $M_w = 7.8$ is triggered at the boundary of the Central and Assam seismic gap and, the probability of the occurrence of an EQ of high magnitude ($M_w > 8.5$) in near future, may be associated with the central seismic gap, which has been reported by Khattri [1999]. Therefore, the entire framework of this study has been divided into two folded objectives: (1) to develop synthetic ground motion based GMPE for the Bihar region considering the central seismic gap and (2) to perform ground response analysis using the synthetically generated ground motion to quantify the amplification of seismic waves in alluvium soil deposit.

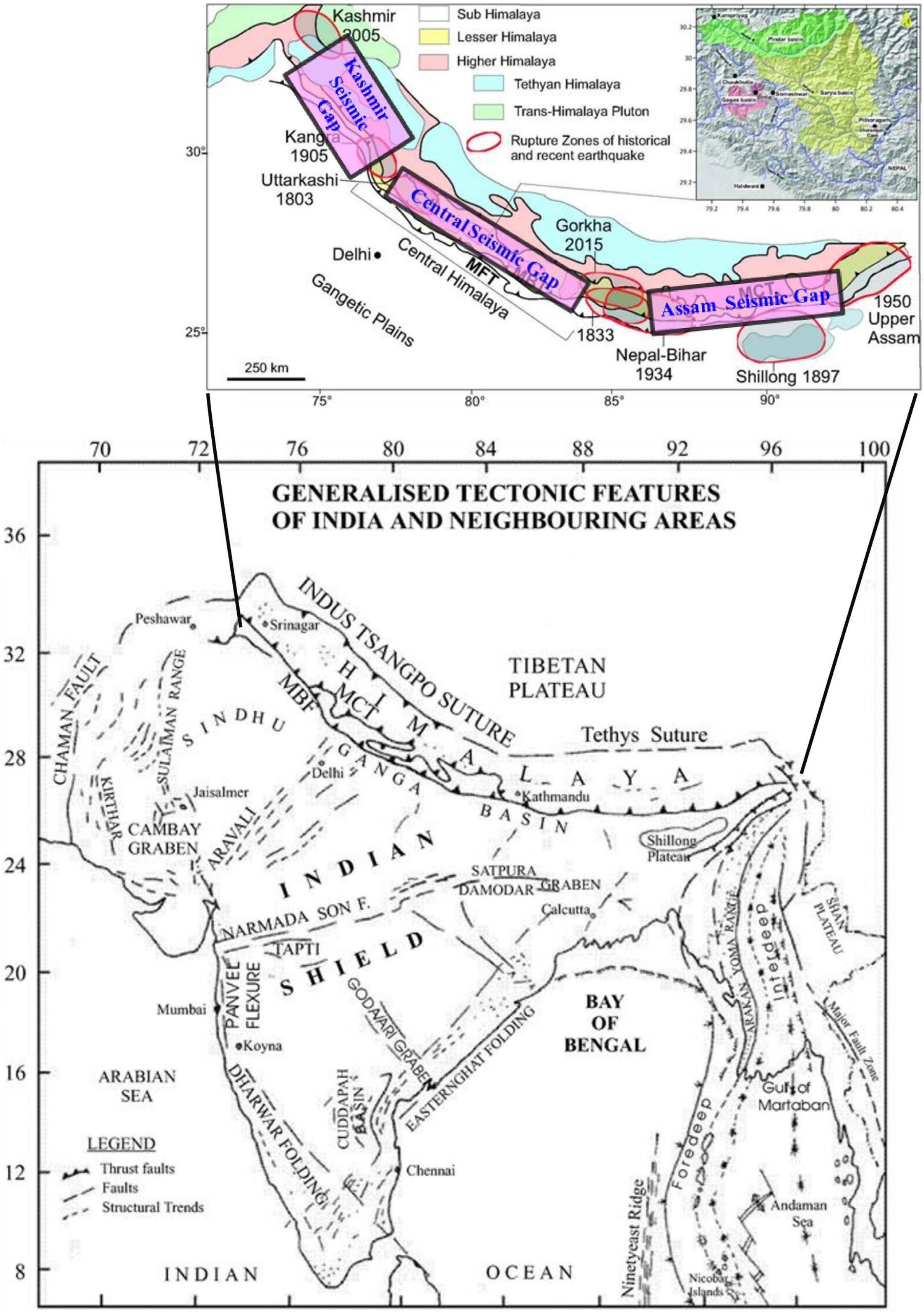

Figure 1. Tectonic feature of India and Nepal region [modified after Parvez et al. 2003].

2. Study Area

Bihar, one of the oldest inhabited places in the world which witnessed the rise of the great Magadha empire, is the Eastern state of India falling between latitudes 24°20'10"N and 27°31'15"N and longitudes 83°19'50"E and 88°17'40"E (shown in Figure 2). The river Ganga which flows across the state separates North Bihar from South Bihar, and also responsible for the deposition of alluvium soil. It also straddles the river Ghaghara, Burhi Gandak, Mahananda, Kosi, Gandak and Son. Most of its area consists of thick alluvium deposited by Ganga and its tributaries whereas, the southern part of the region has crystalline and metamorphic rock deposits. Eight districts of Bihar comes under the seismic zone V, 24 comes under seismic zone IV and 6 comes under seismic zone III, as per the seismic-zonation map of India (IS 1893: 2016); where, seismic zone V possess very high seismic intensity (≥ IX) as per the Medvedev-Sponheuer-Karnik (MSK) scale (mentioned in Figure 2). Bihar lies in between the Indian shield and the Himalayas and constitutes a substantial portion of the Indo-Gangetic plain (IGP) also known as the

Figure 2. Classification of Seismic zones of Bihar.

Himalayan fore-deep. IGP was formed after the upliftment of the Himalayas due to the collision of the Indian and the Eurasian plates [Dewey and Bird, 1970].

2.1 Seismotectonic Feature of Bihar

The study area consists of many tectonically active features such as Main frontal thrust (MFT), Main Boundary thrust (MBT), Main Central thrust (MCT), East Patna fault (EPF), West Patna fault (WPF), Sitamarhi fault (SIF), Munger Saharsa Ridge fault (MSRF), Munger Saharsa Ridge Marginal fault (MSRMF), Malda Kishanganj fault (MKF), Katihar-Nailphamari fault (KNF) and Purnia-Everest lineament (PEL) presented in Figure 3 [Dasgupta et al., 1987; Geological Survey of India (GSI) 2000; Burnwal et al., 2017]. Along with these faults, there are other two faults perpendicular to WPF, aligned in the North-West (NW) direction, falling aside to the Sitamarhi and Siwan [Geological Survey of India, 2000]. The EPF is oriented in a NE-SW direction from Patna in the south to the Nepal border to the

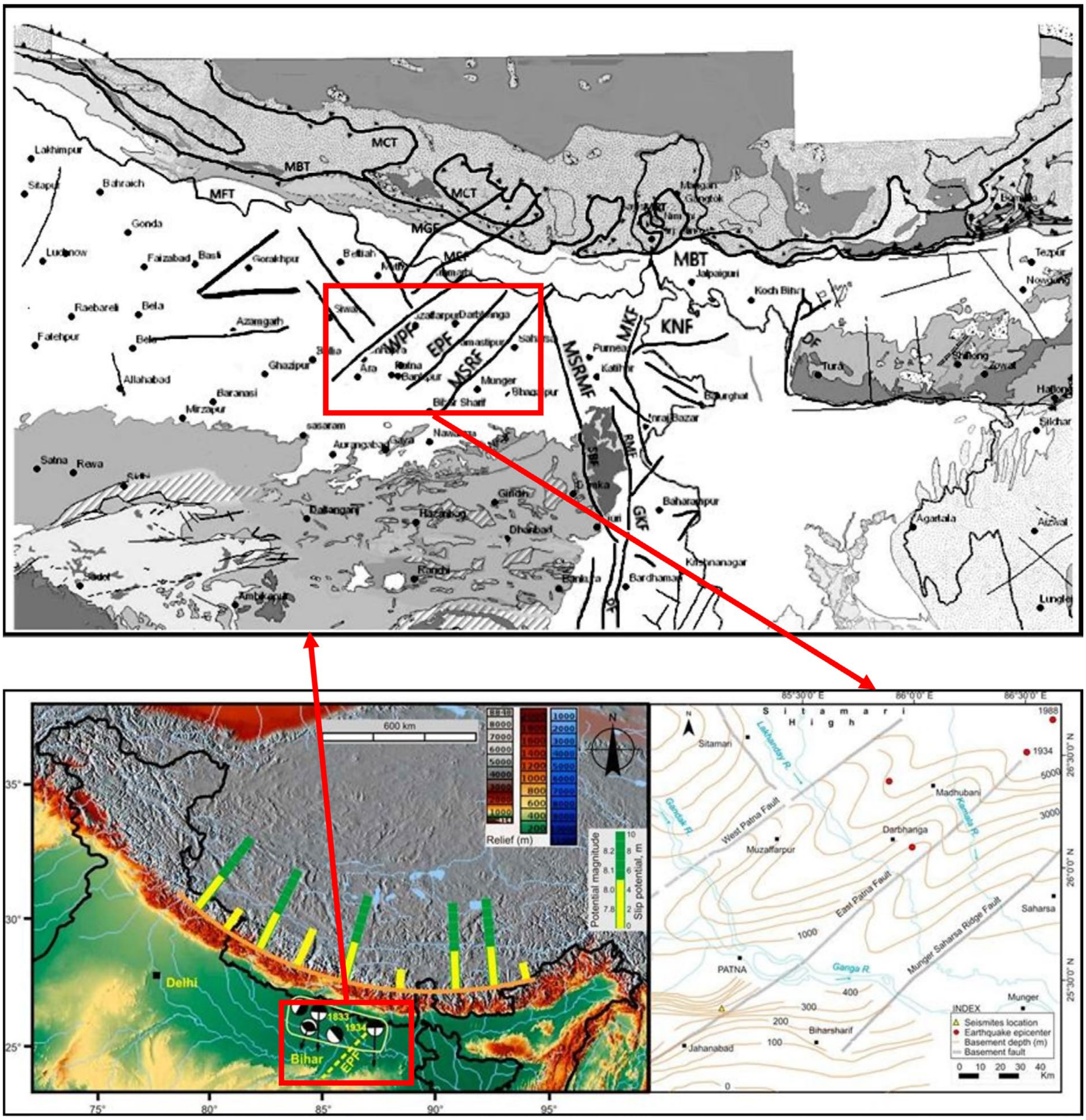

Figure 3. Tectonic features of the region [modified after GSI, 2000 and Verma et al., 2017].

east of Madhubani, shown in Figure 3. WPF and MSRF run almost parallel to it on the left from Arrah to the Nepal border and on the right from Bihar Sharif to Morang in eastern Nepal [Ghosh and Mukhopadhyay, 2013].

Among these, EPF is one of the most active faults since, the several major earthquakes such as 1934 and 1988 earthquakes are associated with this fault and, it can lead to a number of EQs primarily due to interaction with MFT [Anbazhagan et al., 2015; Verma et al., 2017; Banghar, 1991]. Munger-Saharsa ridge denotes the prolongation of the Bundelkhand and Satpura massifs. Further, IGP represents the depressed part of the Peninsular India and contains several hidden east-west directed tectonic features due to narrow MFT [Gansser, 1974; Valdiya, 1976]. The crustal thickness of this region varies from 30 to 45 km and, increasing in the north direction [Choudhury, 1975]. The sediment accumulation rate in north Bihar is very high, ranging from 0.7-1.5 mm/year, as compared to the average sediment deposition rate of 0.2 mm/year due to the web of rivers throughout the region [Joshi and Bhartiya, 1991; Chandra, 1993; Sinha et al., 1996]. The alluvial deposits have a thickness of 1.5-5.0 km, concealing the solid geology of the basement [Quittmeyer and Jacob, 1979]. Such continuous deposition of sediments in a layer, of thickness up to several kilometers, leads to the higher path attenuation [Sinha et al., 2005; Harinarayan and Kumar, 2020].

2.2 Seismicity of Bihar and Adjoining Region

The continental collision of the Indian and Eurasian plates, which are converging at a relative pace of 40-50 mm/year, causing different amplitude of seismicity in the Himalayan region [Bilham, 2004; Hayes, 2017]. The northward under-thrusting of the Indian plate beneath the Eurasian plate causes several EQs of different magnitudes (M_w), ranging from 4.0-8.0, makes this region one of the most seismically dangerous. The seismic activity in the region is broadly related to the strike-slip faulting of shallow nature i.e., less than 70 km with a 15% average fault rupture [Gupta, 2006 and Anbazhagan et al., 2015]. However, in comparison to the Himalayan region, the Bihar region of Indo-Gangetic plain is moderately seismic [Quittmeyer and Jacob, 1979]; though, some devastating EQs of $M_w \geq 6.5$ (Figure 4) in the past, in the study region, indicates high seismically vulnerable region.

The recent 2015 Nepal EQ alone has more than 100 aftershocks of $M_w \geq 3$ [Hayes, 2017], which is also one of the indications of the seismic vulnerability of the region. The source of EQs that causes damage in Bihar region falls under the Bihar-Nepal Himalayan region (Figure 4). Table 1 shows some of the past EQs in the region, caused a lot of destruction in the Bihar region, which have proven the regional devastation.

S. No.	Earthquakes	Date	Time [UTC]	Latitude	Longitude	Magnitude [M_w]	Depth [km]	Fatalities
1	1833 Bihar	26 Aug	18:05:00	NA	NA	7.5	NA	500
2	1934 Bihar-Nepal	15 Jan	08:43:25	26.885° N	86.589° E	8.0	15	10600
3	1988 Bihar-Nepal	20 Aug	23:09:09	26.71° N	86.62° E	6.9	62	1500
4	2015 Nepal (Gorkha EQ)	25 April	06:11:25	28.230° N	84.731° E	7.8	8.2	9000
5	2015 Nepal (aftershock)	12 May	07:05:19	27.809° N	86.066° E	7.3	15	100

Table 1. Major earthquake in Bihar and adjoining area.

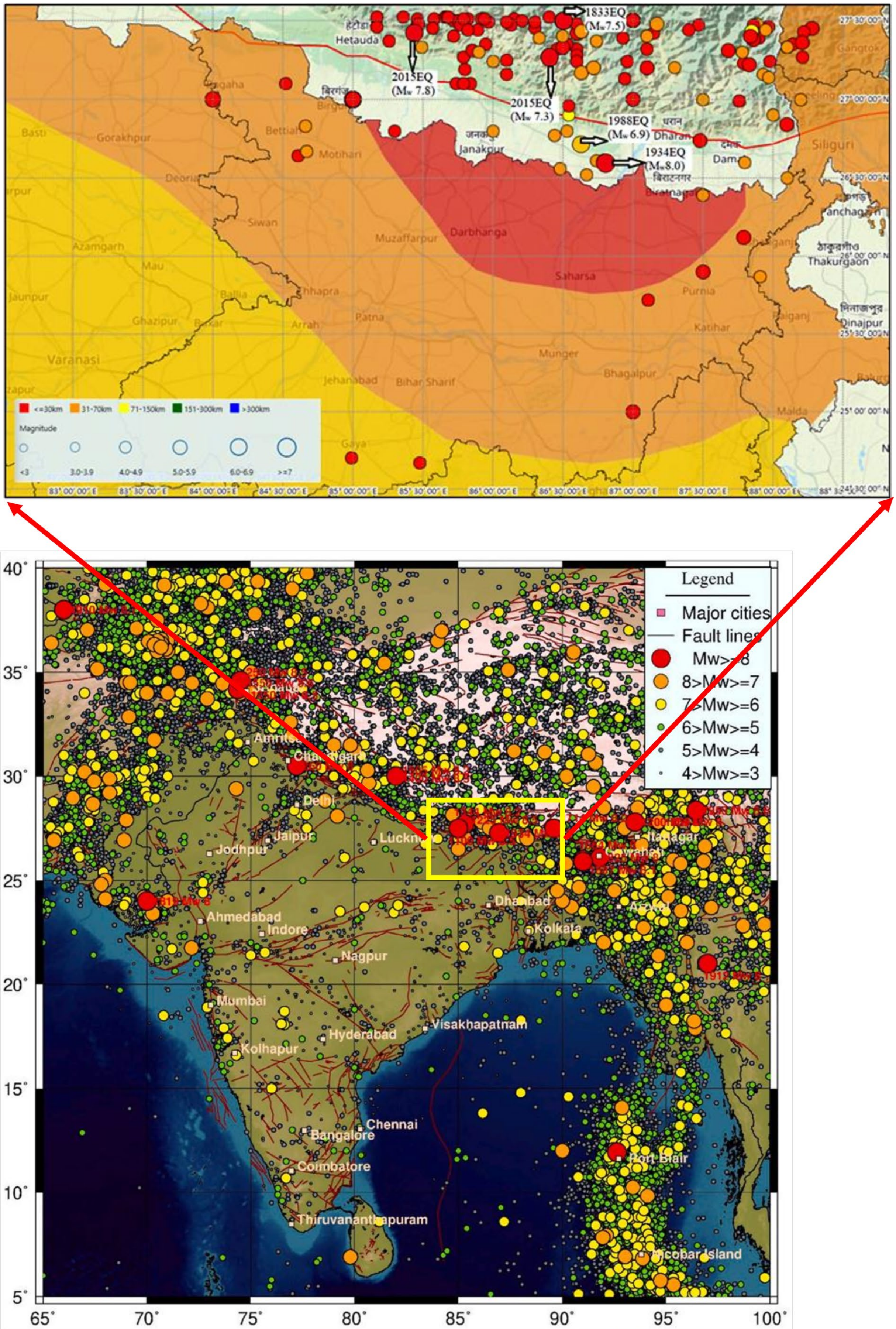

Figure 4. Seismicity of study area [modified after Sreejaya et al., 2022 and Earthquake Catalogue 2023].

3. Insight into existing GMPEs for India

The foundation for the development of regional GMPE for India was set up by Singh et al. [1996]. GMPE model for the plate boundary of the Himalaya region was developed utilizing 86 GM records, obtained using 5 recorded ground motions, from the Kangra array and Shillong array. Singh et al., [1996] have developed the attenuation relationship for Peak Horizontal Acceleration (PHA) and Peak Horizontal Velocity (PHV) considering all of the EQs has similar source characteristics and uniform regional geology. The intensity of EQs (based on MMI scale) was also considered as a representation of the regional site parameters which is later correlated with coefficients of Peak Ground Acceleration (PGA) attenuation to obtain GMPE coefficients. Sharma [1998] has proposed a GMPE relationship for the Himalayan region based on mixed soil conditions, utilizing 66 records from 5 events. These GMPE relationships cannot be utilized for the Probabilistic Seismic Hazard Analysis due to lack of data as well as the absence of standard error term. Later on, Iyengar and Ghosh [2004] modified the correlation, proposed by Sharma [1998], to develop a GMPE for Delhi region. The total 38 records from Sharma's dataset and 23 new records were utilised, considering uncertainty in magnitude as well as in the hypocentral distance, for the earthquake magnitude (M_w) range of 4.0 to 7.0 and $R_{\text{hypo}} \leq 300$ km.

Furthermore, the researchers have utilized the concept of point source model proposed by Brune, [1970] to develop the GMPEs. Using this model, Baruah et al. [2009] developed a GMPE relationship for the north-eastern region, considering GMPE model proposed by Campbell [1985], using 82 events of strong ground motions from 9 stations in the Shillong plateau, of M_w ranging from 2.5 to 5.0. Similarly, Gupta [2010] has proposed a model, for NEHRP site classes B and C, considering only 3 EQ of rupture distance (R_{rup}) ≥ 150 km and M_w ranging from 6.2 to 7.2. A GMPE has also been developed by NDMA [2010] for whole India considering 32-seismotectonic zones and the maximum magnitude of earthquakes in each of the 32 seismotectonic-tectonic zones was assigned using prehistoric data by Kijko and Graham [1999] method [Seeber et al., 1999; Bhatia et al., 1999; Gupta, 2006]. The GMPE relationship, proposed by NDMA [2010], has considered 80000 strong motion data from 38860 events of magnitude range $4.0 \leq M_w \leq 8.5$ and hypocentral distance (R_{hyp}) ≤ 500 km.

Further, the concept of Finite fault modeling was also utilized by several researchers for development of GMPE. Anbazhagan et al., [2013a] have utilized this concept and developed a GMPE for Indian Himalayan region, based on FINSIM model proposed by Beresnev and Atkinson [1998], for $3.0 \leq M_w \leq 8.7$ and $R_{\text{hypo}} \leq 300$ km, after introducing the concept of apparent station. The GMPE model, reported by Anbazhagan et al. [2013a], has been derived from 420 ground motions records obtained from 14 EQs recorded at 30 stations placed at an interval of 10 km. It also include the past seismicity data obtained from the correlation between MMI and surface PGA values proposed by Murphy and O'brien [1977]. Harbindu et al. [2014] also used Finite fault model to develop a GMPE relationship for the Garhwal Himalaya utilizing 78 (3-component) records of 7 EQ events recorded at 16 stations. This GMPE model is based on Boore's [2003a]model and, applicable for $3.5 \leq M_w \leq 6.8$ and $R_{\text{hypo}} \leq 250$ km. Later, Ramkrishnan et al. [2019] have proposed a improved GMPE for the North and Central Himalayas, M_w range $4.1 \leq M_w \leq 7.8$, by incorporating large distance range i.e., extended upto 1560 km; however, the fault mechanism and tectonic environment were not considered.

Further, it was reported that the lack of recorded motions in the Himalayan region was a major obstacle for the development of a reliable GMPE relationship, which has been shorted out by opting the synthetic generation of ground motion by using datasets from other regions of similar seismicity [Bajaj and Anbazhagan, 2019c; Harnarayan and Kumar, 2020]. Sharma and Bungum [2006] have developed a GMPE for the Himalayan region using datasets of adjoining region considering similar seismic features in both the regions. For this, 175 recorded motions from 14 events ($4.5 \leq M_b \leq 7.2$) of the Himalayan region and 9 events ($6.0 \leq M_b \leq 7.4$) from the European region were utilized to develop a relationship for M_w 5.6 to 7.6 and $R_{\text{hypo}} \leq 200$ km. In a similar fashion, Sharma et al. [2009] utilized 201 records, obtained from six EQs ($5.5 \leq M_w \leq 6.8$) of the Himalayan region and 10 EQs ($5.9 \leq M_w \leq 6.6$) of the Zagros region, to develop GMPE for the magnitude range of M_w 5.0 to 7.0 and $R_{\text{hypo}} \leq 100$ km. Further, Sharma et al. [2009] have used Iranian data considering tectonic similarity of both the regions reported by Talebian and Jackson [2004]. But, the similarity of both regions is still questionable regarding parameters like creep, under-thrusting, etc. [Ni and Barazangi, 1986; Jackson, 2002] and thus, the model proposed may not be reliable for the Indian region as it utilized 143 records, out of 201, from Iran. Raghukanth and Iyengar [2007] derived an empirical GMPE relationship for Peninsular India, using Atkinson and Boore [1995] model, by dividing the whole Peninsular India into three regions based on their Quality factor (Q). The work was compiled after generating 10100 datasets from 900 synthetic ground motions using the point source model of Brune [1970]. The local site effect was also

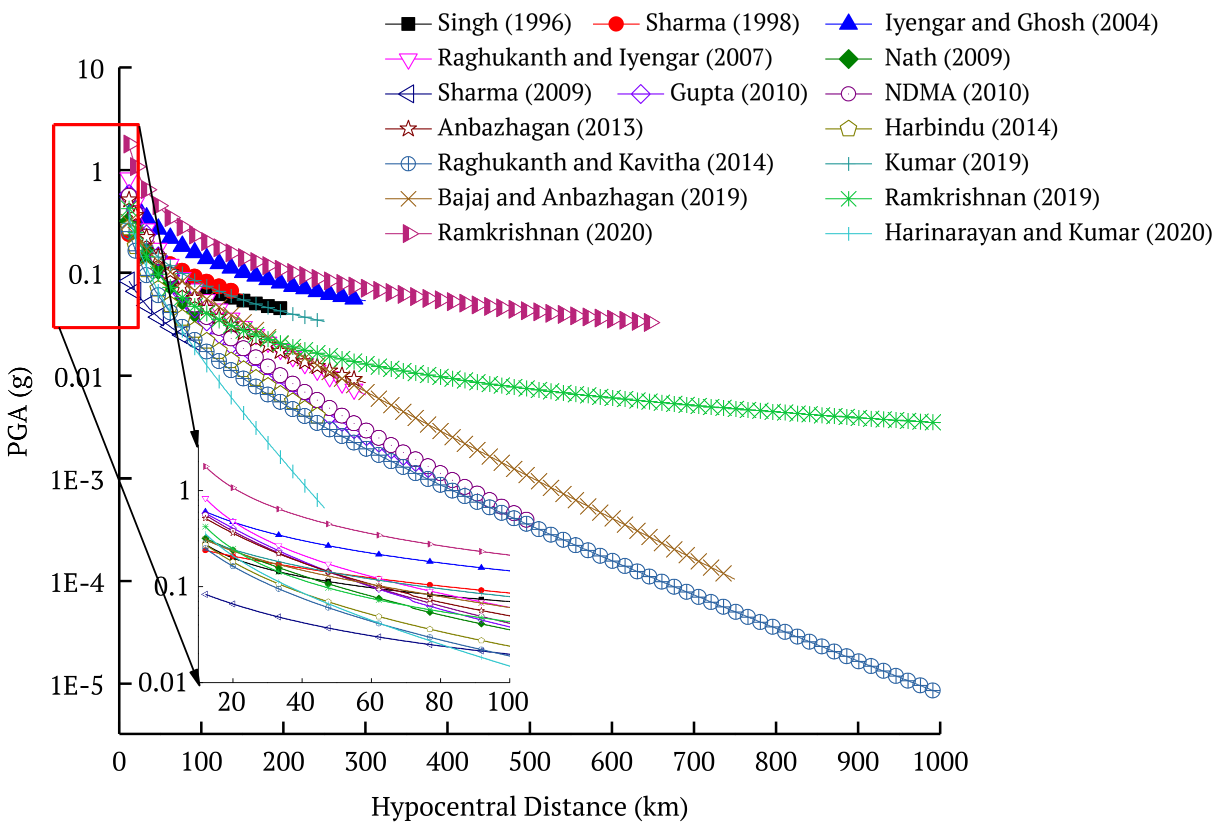

Figure 5. Variations in PGA with hypocentral distance based on different GMPE models for the Himalayan region for $M_w = 6.8$.

incorporated during the analysis by Raghukanth and Iyengar [2007]. Nath et al. [2005] have used the synthetic ground motion for the generation of GMPE for north India wherein, the source and site amplification was performed using HVSR (Horizontal to Vertical Spectral Ratio) and GNIV (Generalized Inversion method) technique [Lermo and Chávez-García, 1993 and Nath et al., 2002, 2003]. Further, Nath et al. [2009] have proposed a relationship with an improvement, over the previously developed models, in terms of site amplification [Nath et al., 2008b, a]. The study was based on the Finite fault stochastic model (EXSIM), proposed by Motazedian and Atkinson [2005], which incorporate the spectral amplitude in the analysis based on the convolution theorem [Nath et al., 2005; Boore, 1983]. Harinarayan and Kumar [2020] have also proposed a GMPE based on synthetically generated earthquake for north India after incorporating NEHRP-based site classes A/B, C, D, and E.

Moreover, the summary of GMPE model developed for different Indian region, are compiled in Table 2, which also indicates that the GMPE for Bihar region is scanty. Bihar region, a region of Indo-Gangatic plain, is situated near the foothills of Himalayas consisting alluvium soils deposit. Therefore, an effort has been made by NDMA [2010] and Raghukanth and Kavitha [2014] to develop GMPE for Indo-Gangetic plain by considering the source parameter and geometric attenuation similar to the Himalayan region, which might be erroneous. Therefore, estimating the bedrock ground motion of different magnitudes for Bihar region, incorporating the regional parameters, are utmost important.

Figure 5 shows the variations of PGA with hypocentral distance for $M_w = 6.8$ using existing GMPE models, mentioned in Table 2. In order to see the variations in the existing GMPE models with hypocentral distance, the model which is associated with the Joyner-Boore distance (R_{jb}), has been brought to a scale of hypocentral distance using Scherbaum et al. [2004] correlation. From Figure 5, it is noticed that each model shows different variations of PGA with distance, though it is developed for the Himalayan and their adjoining region. Therefore, it is quite difficult to choose one GMPE model which can be reliable to use for region-specific microzonation or seismic hazard studies. Hence, the generation of a new GMPE has been attempted in this study based on the synthetically generated ground motion.

S. No.	GMPE Model	Magnitude Range	Distance Range [km]	Datasets	Region-specific
1	Singh et al. [1996]	5.5-6.8	$R_{hyp} \leq 200$	86 @ 5*	Pan Himalaya
2	Sharma [1998]	5.5-6.8	$R_{ep} \leq 150$	66 @ 5	Pan Himalaya
3	Iyengar and Ghosh [2004]	4.0-7.0	$R_{hyp} \leq 300$	61	Northern India
4	Nath et al. [2005]	3.0-8.5	$R_{hyp} \leq 100$	80 + SM	Sikkim Himalaya
5	Sharma and Bungum [2006]	4.6-7.6	$R_{hyp} \leq 200$	14 Himalayan + 9 European	Northern Himalaya
6	Raghukanth and Iyengar [2007]	4.0-8.0	$R_{ep} \leq 300$	10100 @ 900	Peninsular India
7	Sharma et al. [2009]	5.0-7.0	$R_{hyp} \leq 100$	201 @ 16	Northern Himalaya
8	Nath et al. [2009]	4.8-8.1	$R_{rup} \leq 100$		Guwahati
9	Baruah et al. [2009]	2.5-5.0	$R_{ep} \leq 140$	@ 82EQ	Shillong
10	Gupta [2010]		$R_{rup} \leq 150$	56 @ 3	Indo-Burma
11	NDMA [2010]	4.0-8.5	$R_{hyp} \leq 500$	80,000 @ 38860	Pan India
12	Anbazhagan et al. [2013a]	3.0-8.7	$R_{hyp} \leq 300$	30	Himalayan region
13	Harbindu et al. [2014]	3.0-6.8	$R_{hyp} \leq 250$	78 @ 7	Garhwal Himalaya
14	Raghukanth and Kavitha [2014]	3.4-7.6	$R_{hyp} \leq 1000$	236@62	Active Himalayan region
15	Ramkrishnan et al. [2019]	4.1-7.8	$R_{hyp} \leq 1560$	278 @ 33	North & Central Himalaya
16	Kumar et al. [2019]	5.0-6.8	$R_{hyp} \leq 250$	116 @6	Uttarakhand
17	Bajaj and Anbazhagan [2019b]	4.0-9.0	$R_{hyp} \leq 750$	520 @ 78	Himalayan region
18	Harinarayan and Kumar [2020b]	3.5-7.8	$R_{ep} \leq 250$	20,000	North India

* 86@5 denotes 86 records originated from 5 events.
R_{rup} = rupture distance; R_{hyp} = hypocentral distance; R_{ep} = epicentral distance.

Table 2. Compendium of GMPEs for the Indian region.

4. Generation of Synthetic Ground Motion

The generation of synthetic ground motion provides an effective way to develop GMPEs for the regions having sparse ground motion records [Boore and Atkinson, 1987; Nath et al., 2009; Raghukanth, 2008a,b]. In the present study, due to the unavailability of recoded EQ motion (i.e., due to the unavailability of recording stations in the Bihar region) during past EQ events, the stochastic seismological model, proposed by Boore [1983], has been adopted to generate the synthetic ground motion. Prior to the generation of GMPE using regression analysis for 5% damped response spectrum, the various regional model parameters were required for the ExSIM code. Figure 6 presents the flow chart, which is used in this study, to develop a GMPE-based synthetically generated ground motion for seismic GRA.

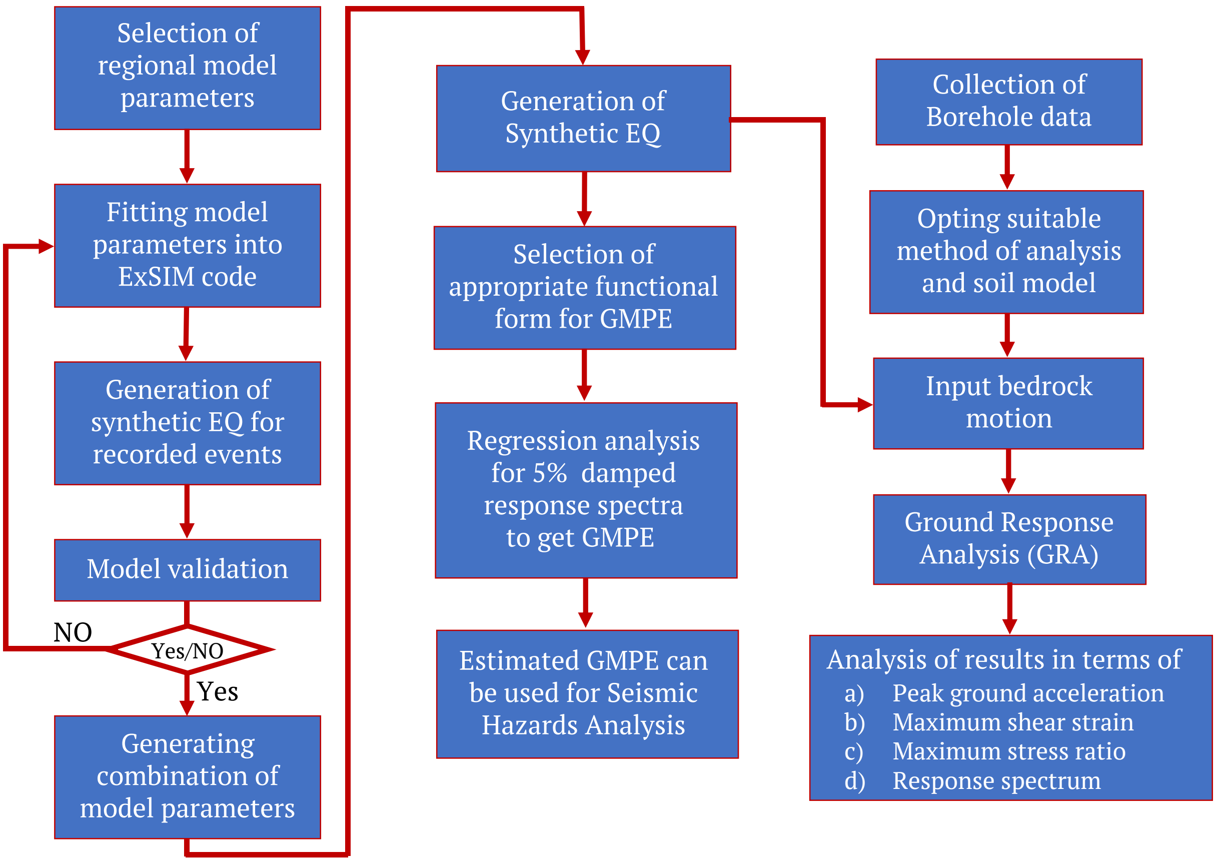

Figure 6. Flow chart for the development of synthetic ground motion to perform GRA.

4.1 Seismological Model Parameters

Boore and Atkinson [1987] developed a stochastic seismological model to simulate the ground motion considering point source, the concept was further utilized by several researchers [Raghukanth, 2008]. Improvement in the research over time helped the researchers to overcome the problems in capturing the effect of rupture propagation and directivity associated with the point source model through the use of the finite fault approach. The finite fault approach proposed by Hartzell [1978], splits the rupture region into many sub-faults, each of which is modelled as an individual point source and their summation with proper time delay constructs the main event. This significant improvement leads to the wide use of finite fault approach for ground motion simulation [Kanno et al., 2006; Bajaj and Anbazhagan, 2019a; Ramkrishnan et al., 2020]. In this study, synthetic ground motion is generated using EXSIM model, established by Motazedian and Atkinson [2005], which is based on the notion of dynamic corner frequency and a modified version of FINSIM model proposed by Beresnev and Atkinson [2002]. For the generation of synthetic ground motion, the regional generic physical constants such as average crustal density (ρ) value = 2.8g/cc and crustal shear wave velocity (β) = 3.4 km/sec are chosen for this study as per Singh and Khan [2021] and Mukhopadhyay and Kayal [2003], respectively. Since, these physical parameters do not contribute any substantial uncertainty to the model, the variation of these physical parameters were not taken into the account and hence, kept a constant value [Atkinson and Boore, 2006].

Further, Wells and Coppersmith relationship [Wells and Coppersmith, 1994] is used to calculate the rupture length and rupture width for a given moment magnitude (M_w). The rupture begins at the hypocenter is considered centre of the main fault and, extends radially to the additional sub-faults with a rupture propagation velocity of 0.8β [Atkinson and Boore, 2006]. The initial energy produced by the seismic wavefront is distributed across an expanding region, as the wavefront advances away from the source, resulting in the declination of wave strength in the form of amplitude reduction. This loss is represented in terms of geometric spreading which can be accounted either in a bilinear or in a trilinear functional form. Several researchers in past have used the bilinear form, proposed by Singh et al. [1999] for the Himalayan region, to account the strength loss due to the spreading of waves [Iyengar and Raghu Kanth, 2004; Raghukanth and Iyengar, 2007; Singh et al., 2016; Harinarayan and Kumar, 2020]. However, at a higher distance range, an incremental shift in Fourier amplitude is observed due to post-critical reflection by the Moho and Conrad discontinuities [Atkinson 2004]. Therefore, the trilinear variation of geometric spreading, proposed by Boore [2003b], has been used in this study (shown in Table 3). Similar consideration has been made by Bajaj and Anbazhagan [2019b] for the development of GMPE of Bihar-Nepal Himalaya region. The Bihar-Nepal Himalaya region consists of moderately aged rocks i.e., Pleistocene age to recent time [Upreti, 1999], resulting in the moderate value of kappa which controls the behaviour of Fourier amplitude spectrum at high frequency. The kappa value for the study region (see Table 3) is considered from Bihar-Nepal Himalayan region after Bajaj and Anbazhagan [2019b] whereas, strike and dip for Bihar region is opted in the range of 20° to 48° and 2° to 27°, respectively [NDMA, 2010]. Further, the stress-drop after Kayal [2008] and Raghukanth and Kavitha [2014] has been considered for this study. The stress drop, is mainly used to describe the amplitude of acceleration spectrum in the near field area, regulates the high-frequency radiation in the epicentral region depending on the rupture velocity. Generally, a low value of stress drop has been observed in case of high rupture velocity [Manighetti et al., 2007].

Further, the quality factor, ratio of stored energy to dissipated energy, has been introduced to quantify the loss of relative energy per oscillating cycle. It is inversely related to the attenuation factor and is also sensitive to the fluid movement and grain boundary friction [Fukao and Obayashi, 2015]. For the present study, the regional quality factor reported by Harinarayan and Kumar [2020] has been considered, presented in Table 3. Bilham [2015] highlighted about the chance of the occurrence of EQs of greater magnitude ($M_w > 8.0$) and, therefore, the synthetic ground motions were generated for M_w ranging from 4.0 to 8.5 considering R_{hyp} range 10 km-300 km with an unit step of 0.1 and 10 km, respectively. The path duration function is another key element in the modelling of ground motion whereas, the total duration is equal to the sum of the source and path durations [Boore, 2003a]. Moreover, it is difficult to construct a new duration model due to a paucity of collected data. Thus, in this investigation, the ground motion was simulated using the duration model, mentioned in Table 3, developed by Atkinson and Boore [2006].

S. No.	Parameters	Values	Reference
1	Crustal density (ρ)	2.8 g/cc	Singh and Khan [2021]
2	Crustal Shear wave velocity (β)	3.4 km/sec	Mukhopadhyay and Kayal [2003]
3	Rupture propagation velocity	0.8β	Atkinson and Boore [2006]
4	Geometric spreading	$G = \begin{cases} R^{(-1.11)}; \text{for } R \leq 40 \text{ km} \\ 40^{(-1.11)}\left(\frac{R}{40}\right)^{(0.02)}; \text{for } 40 \text{ km} < R \leq 160 \text{ km} \\ R40^{(-1.11)}\left(\frac{160}{40}\right)^{(0.02)}\left(\frac{R}{160}\right)^{(-0.45)}; \text{for } R > 160 \text{ km} \end{cases}$	Bajaj and Anbazhagan [2019b]

S. No.	Parameters	Values	Reference
5	Kappa	0.015±10%	Bajaj and Anbazhagan [2019b]
6	Quality factor	$Q = 105 \pm 11f^{0.94\pm0.09}$	Harinarayan and Kumar [2020b]
7	Duration model	$T_d = \begin{cases} 1/f_c\text{; for } R_h < 10\text{ km} \\ 1/f_c + 0.16R_h\text{; for } 10\text{ km} \le R_h < 70\text{ km} \\ 1/f_c - 0.03R_h\text{; for } 70\text{ km} \le R_h < 130\text{ km} \\ 1/f_c + 0.04R_h\text{; for } R_h \ge 130\text{ km} \end{cases}$	Atkinson and Boore [2006]
8	Magnitude (M_w)	4.0 to 8.5	Anbazhagan et al. [2015]; Burnwal et al. [2017]; Srivastava et al. [2015]
9	Hypocentral distance	10 km to 300 km	
10	Stress Drop	50 to 200 bars	Kayal [2008]; Raghukanth and Kavitha [2014]
11	Strike	312° to 340°	Jaiswal and Gupta [2020]
12	Dip	2° to 27°	NDMA [2010]
13	Faulting mechanism	Strike-Slip	Paudyal [2010, 2011]; Chandra [1978]

Table 3. Input parameters used for simulating the ground motion.

4.2 Model Validation

To test the ability of synthetic ground motions to forecast PGA, a comparison is made in terms of PGA obtained from synthetic ground motion with the recorded ground motions along with the spectral acceleration and Fourier amplitude spectrum. Figure 7(a-b) presents the comparison of acceleration time histories of recorded and synthetically generated data at the bedrock level. The recorded ground motion data at the bedrock level is very limited in the study region, which is creating difficulties in the generation and validation of GMPE. Therefore, the records of Sikkim EQ motion at bedrock level, near the boundary of the Nepal-Bihar region, have been chosen for the validation of results obtained from EXSIM model. It can be observed from Figure 7(a-b) that the simulated ground motions are very close to the recorded motions. However, the marginal difference between synthetic ground motion and the recorded ground motions was observed, in the Figure 7(a-b), which is attributed to lack of the incorporation of realistic soil behaviour into the stochastic seismological model. Similar responses were reported by Anbazhagan et al. [2013a] during the generation of synthetic ground motion. Figure 7(c-d) depicts the comparison between the spectral acceleration obtained from the recorded motions and synthetic ground motions for the acceleration time histories reported in Figure 7(a-b). Since most of the structures are associated with their natural period, the spectral acceleration can be a better descriptor of seismic hazard and directly applicable to the design of structures [Kumar et al., 2018a]. The natural period of most of the structures is generally less than 3s, which is also reflected by both recorded motions and synthetic ground motions. Based on the results of spectral acceleration, in Figure 7(b-c), it can be stated that the response of simulated ground motions are very close to the recorded motion of similar moment magnitude and can provide a similar response as that of recorded motion. However, the marginal difference, observed in Figure 7(b-c),

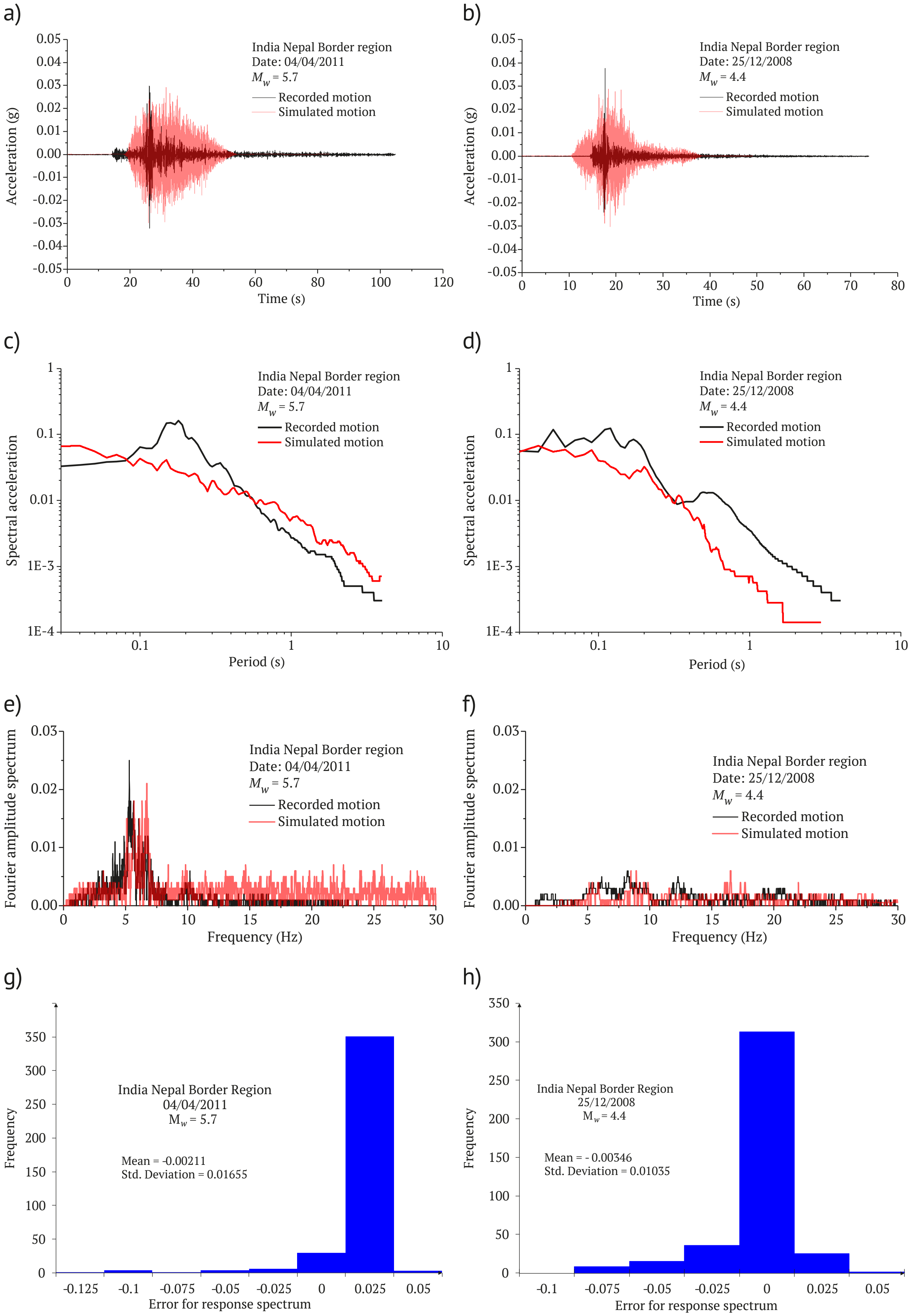

Figure 7. **(a-b)** comparison of simulated and recorded ground motion **(c-d)** comparison of simulated and recorded spectral acceleration **(e-f)** comparison of simulated and recorded Fourier amplitude spectrum, for the mentioned acceleration time histories **(g-h)** error vs frequency plot for the spectral acceleration.

might be associated with the selected ground motion parameters for synthetic ground motion generation. Figure 7(c-d) indicates that the variations on spectral acceleration along with period obtained from both recorded motions and synthetic ground motions are in the very narrow range of deviation and thus, the adaptation of the generation of synthetic motion is justified. Similar responses have been reported by the Anbazhagan et al. [2013]. Figure 7(e-f) shows the variations Fourier amplitude spectrum obtained from recorded motions and synthetic ground motions of the acceleration time histories reported in Figure 7(a-b). These results also indicate that the synthetic ground motions are capable to produce a similar response as that of recorded motions. Thus, overall it can be stated that the marginal difference in the results of synthetic ground motions from the recorded motions, as shown in Figure 7(a-f), is mainly due to the ground motion parameters used in the generation of synthetic ground motions, which might not reflect the exact feature source, site and path function as that of recorded motions. Figure 7(g-h) presents the plot of error against frequency corresponding to the response spectrum shown in Figure 7(c-d), which shows a clear evident that the maximum error corresponds to zero error. The means and standard deviations for each plot are also provided and it can be observed that the mean value of the mentioned event is close to zero. Similar findings were also reported by Anbazhagan et al. [2013a]. Further, based on the results of recorded and simulated ground motions presented in Figure 7(a-f) for all of the apparent stations, it can be stated that the synthetically generated ground motions through EXSIM are capable to predict the recorded data of EQs. Further, these model parameters, shown in Table 3, are used to generate the synthetic ground motion for the study area. The combinations of these model parameters have been formed based on the Latin Hypercube Sampling Technique [Mckay et al., 2000]. The location of events is designed to capture the source finiteness and to cover the whole epicentral region, based on the concept of apparent station [Anbazhagan et al., 2013b]. The apparent stations are distributed in such a way that the successor apparent station will be 10 kilometres apart from its predecessor station, with an azimuth difference of 12 degrees. A total of 500 synthetically generated EQs utilizing the above model and concept are used for further analysis.

4.3 Functional form of GMPE

Functional form of GMPE plays a critical role in reflecting the nature of the model and in reducing the epistemic uncertainty associated with the model [Bajaj and Anbazhagan, 2018]. GMPEs can be represented in a simple quadratic form or complex form. Atkinson and Boore [1995] tested a simple quadratic model for the hazard calculation which was later adopted by many researchers [Raghu Kanth and Iyengar, 2007; Harbindu et al., 2014]. Many such studies have also adopted the log-log form of relation proposed by Campbell [1981)] either directly or after some modification [Anbazhagan et al. 2013a; Kumar et al. 2017, 2019; Ramkrishnan et al. 2020]. However, these functional forms do not consider the magnitude scaling of the EQs. The functional form chosen for developing a regional GMPE should also be checked for its suitability in that particular region. Bajaj and Anbazhagan [2018] have highlighted its importance and also proposed the best-suited GMPE for the Himalayan region considering the effect of magnitude scaling. The functional form used for regression, in the present study, takes care the attenuation of seismic waves, saturation and dependence of magnitude, with a hinge point of $M_w = 6$. However, it does not account the effect of fault type, site response, directivity and faulting depth due to the lack of defined pattern and orientation of the study area. The functional form suggested by Bajaj and Anbazhagan [2018], shown in Eq. (1) and Eq. (2) which is best suited for the Bihar region, is used for shaping GMPE.

$$\ln y = C_1 + C_2(M_w - 6) + \ln R\,[C_3 + C_4(M_w - 6)] + C_5 R + \varepsilon;\ \text{for } M_w < 6 \tag{1}$$

$$\ln y = C_1 + C_2(M_w - 6) + C_3(8.5 - M_w) + \ln R\,[C_4 + C_5(M_w - 6)] + C_6 R + \varepsilon;\ \text{for } M_w \geq 6 \tag{2}$$

where y represents spectral acceleration (g), M_w is moment magnitude, R is the hypocentral distance (km), C_1 to C_6 are the coefficients of regression and ε represents the standard error associated with the equation. The form also takes care of the squared magnitude term for larger events, constrained to a maximum magnitude of 8.5. the coefficients from C_1 to C_6 were determined after the nonlinear least square regression method [Boore and Joyner, 1982]. Regression has been carried out for 500 EQs dataset, with a distance range of up to 300 km. The value of

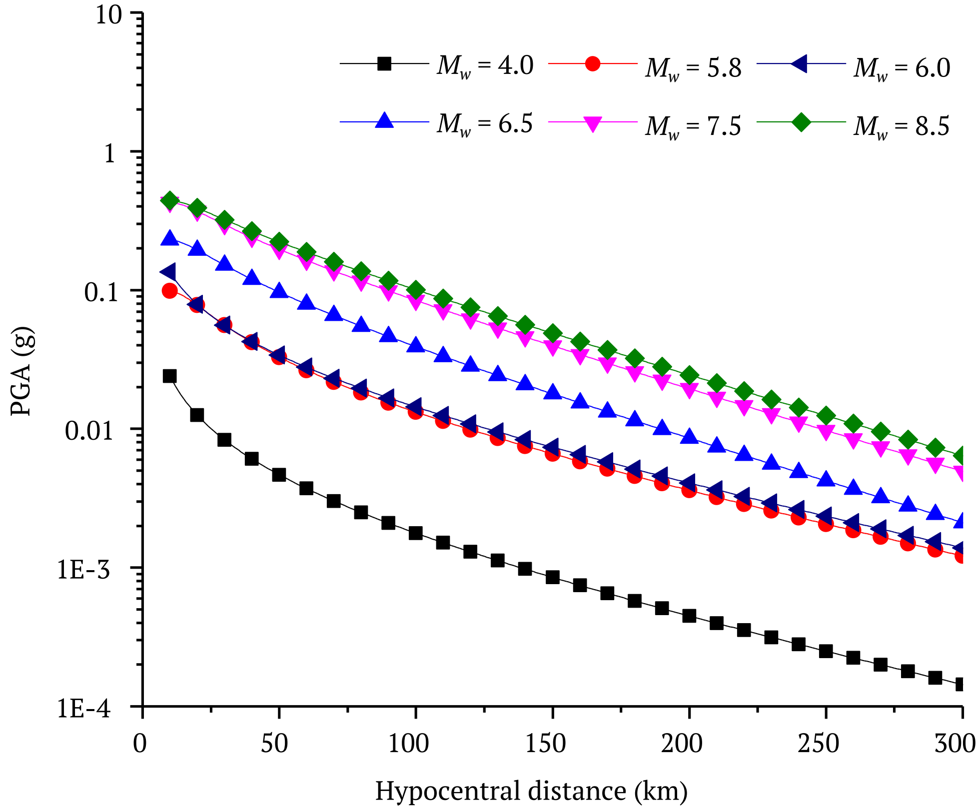

Figure 8. Variation of PGA with hypocentral distance from different moment magnitude using developed GMPE in this study.

coefficients C_1 to C_6 for $M_w < 6$ and $M_w \geq 6$ are given in Table 4 and Table 5, respectively, for the period of 0 s to 10 s. PGA and spectral acceleration, at different frequencies of interest, may be calculated using Eq. (1) and Eq. (2), utilizing the coefficients (C_1 to C_6, mentioned in Table 4 and Table 5), corresponding to any known value of M_w and R. Since the attenuation relationship play a significantly important role in the seismic design of structures, the development of synthetic ground motion based GMPEs can be the best option if recorded ground motion data are not available. Figure 8 shows the variations of PGA with hypocentral distance for different M_w using the developed GMPE model in this study, reported in Eq. (1) and Eq. (2). It can also be noticed that the EQ of lesser magnitude attenuates faster (say, for $M_w = 4.0$, the attenuation rate for the given range of distance is nearly 165%) in comparison to the high magnitude EQs (say, $M_w = 8.5$, the attenuation rate for the given range of distance is nearly 82%), due lesser energy content involves with the lesser magnitude and vice versa. The results found in this study are consistent with the results reported by the researchers, mentioned in Table 2.

Period (s)	C1	C2	C3	C4	C5	Standard Error (ε)
0.00	−0.41329	0.681798	−0.65588	0.079378	−0.00808	0.390345
0.01	−0.35087	0.668772	−0.65748	0.080083	−0.00815	0.4009
0.02	−0.10797	0.630333	−0.63672	0.076731	−0.00872	0.446937
0.04	0.299377	0.693921	−0.63278	0.057906	−0.00891	0.447002
0.07	0.367809	0.747885	−0.62712	0.050601	−0.00867	0.406162
0.10	0.232686	0.807357	−0.59894	0.046382	−0.00865	0.380564
0.12	0.236621	0.894754	−0.61345	0.035863	−0.00838	0.366366

Period (s)	C1	C2	C3	C4	C5	Standard Error (ε)
0.15	0.208936	0.958176	−0.62061	0.033741	−0.0082	0.35665
0.20	0.086203	1.048216	−0.61548	0.034814	−0.00794	0.333016
0.30	−0.12441	1.263933	−0.61087	0.027301	−0.00775	0.307642
0.40	−0.27453	1.455287	−0.60807	0.027107	−0.00753	0.301153
0.50	−0.42399	1.571108	−0.60483	0.033927	−0.00732	0.2935
0.70	−0.70838	1.838225	−0.5941	0.034788	−0.00713	0.281744
1.00	−0.97126	2.135959	−0.61001	0.030179	−0.00682	0.255651
1.50	−1.60564	2.327294	−0.59985	0.044419	−0.00666	0.222857
2.00	−2.34045	2.247463	−0.54867	0.087015	−0.00648	0.208709
4.00	−3.80728	2.230202	−0.53889	0.116321	−0.00627	0.19211
6.00	−4.85647	2.084996	−0.52396	0.141412	−0.00621	0.196045
8.00	−5.55332	1.991053	−0.51535	0.152842	−0.00624	0.200437
10.00	−6.01593	1.94994	−0.5216	0.155181	−0.0062	0.200808

Table 4. Regression coefficients for $M_w < 6$.

Period (s)	C1	C2	C3	C4	C5	C6	Standard Error (ε)
0.00	1.037585	−0.4392	−0.29493	−0.42091	0.071113	−0.0124	0.543092
0.01	1.091624	−0.44076	−0.2944	−0.42075	0.071016	−0.01247	0.54913
0.02	1.39839	−0.44492	−0.28887	−0.41989	0.072399	−0.01288	0.583492
0.04	1.708259	−0.38354	−0.28299	−0.39799	0.063854	−0.01319	0.593199
0.07	1.787662	−0.3872	−0.28657	−0.39175	0.064735	−0.01298	0.569073
0.10	1.694881	−0.32971	−0.287	−0.38508	0.054822	−0.01271	0.552312
0.12	1.68504	−0.36816	−0.29249	−0.38858	0.060696	−0.01261	0.537736
0.15	1.627215	−0.36959	−0.29014	−0.39606	0.062178	−0.01242	0.529429
0.20	1.45302	−0.33722	−0.29689	−0.38178	0.054873	−0.01225	0.517068
0.30	1.141878	−0.30802	−0.29231	−0.37825	0.054596	−0.01198	0.500628
0.40	0.932603	−0.28178	−0.29516	−0.37142	0.049487	−0.01179	0.495183
0.50	0.838298	−0.30209	−0.3057	−0.37508	0.05134	−0.01162	0.488861
0.70	0.561165	−0.2853	−0.31488	−0.36377	0.046976	−0.01142	0.47581
1.00	0.296669	−0.26223	−0.32193	−0.37054	0.046519	−0.01115	0.470461
1.50	−0.07446	−0.2727	−0.36853	−0.33479	0.038446	−0.01105	0.468097
2.00	−0.27761	−0.27444	−0.40674	−0.32114	0.031714	−0.01088	0.457393
4.00	−0.73916	−0.35011	−0.53227	−0.2938	0.036901	−0.01085	0.449912
6.00	−1.13814	−0.31821	−0.6149	−0.29608	0.03578	−0.01048	0.442004
8.00	−1.49916	−0.25385	−0.65726	−0.31042	0.0387	−0.0103	0.441448
10.00	−1.94143	−0.15679	−0.67241	−0.31108	0.040858	−0.01023	0.440218

Table 5. Regression coefficients for $M_w \geq 6$.

4.4 Comparison of estimated GMPE from the existing GMPEs

For the validation of the developed GMPEs of any region, the recorded ground motion data in that region during past seismic activities would give the best suitable GMPE. Due to the unavailability of recorded ground motions at the bedrock level as well as at the surface level in the Bihar region, the proposed GMPE, in this study, has been compared with the peer-reviewed past GMPEs applicable to the Himalayan region. A moment magnitude (M_w) of 4.0 and 5.8 have been chosen for $M_w < 6$ (shown in Figure 9a-b) whereas, another of $M_w = 6.8$ and 8.5 have been chosen for $M_w \geq 6$ (shown in Figure 9c-d) to present the variations of estimated GMPE. Out of all existing GMPEs in India, only seven were found to be applicable for the Bihar region and, a relative comparison of these GMPEs with the proposed model in this study are presented in Figure 9(a-d). Based on the results presented in Figures. 9(a-d), it can be noticed that although, the estimated GMPE can predict the different value of PGA in comparison with the other GMPEs for given M_w and R_{hyp}, the estimated GMPEs follow a similar trends of variation like the other GMPEs. Figure 9(a) shows the variations in PGA, for $M_w = 4.0$, and it can be noticed that the present study GMPE showing similar response as that of existing GMPEs; however, the present study GMPE is very close to the GMPE reported by Anbazhagan et al. [2013a)] for the hypocentral distance < 150 km. It can also be observed that PGA obtained from the GMPE model reported by [NDMA, 2010] is very close to the present study model for the hypocentral distance greater than 100 km. Further, the Anbazhagan et al. [2013a] model predict the higher value of PGA, in comparison to the PGA obtained from the estimated GMPE, beyond a hypocentral distance of 150 km. This might be due to the path and site characteristics used by Anbazhagan et al. [2013a]. It can also be noticed that in comparison to the present study GMPE for $M_w = 4.0$, the value of PGA based on the GMPEs reported by Anbazhagan et al. [2013a] and Bajaj and Anbazhagan [2019b] was observed to be lesser. Figure 9(b) presents the variations of PGA, for $M_w = 5.8$, and it can be noticed that the present study GMPE is very close to GMPE reported by NDMA [2010] for hypocentral distance > 100 km. Figure 9(c) presents the variations of PGA, for $M_w = 6.8$, and it can be observed that the present study GMPE is very close to GMPE reported by NDMA [2010] for hypocentral distance > 50 km. The recorded PGA of 2015-Sikkim EQ ($M_w = 6.8$) at bedrock level as well as the soil-site level have been included in Fig. 9c, which also highlights the importance as well as the requirement of the development of region-specific GMPE at bedrock level as well as the soil-site level, since each region contains different geology and tectonic features than the other. Figure 9(d) present the variations of PGA, for $M_w = 8.5$, reflects that the present study GMPE is very close to GMPE reported by Raghukanth and Kavitha [2014] for hypocentral distance < 150 km, which manifests the importance of regional seismicity and associated regional strong motion parameters.

The proposed GMPE is significantly different than the GMPE reported by Singh et al. [1996] and Sharma [1998] which has considered similar geology as that of Himalayan region. Moreover, Singh et al. [1996] and Sharma [1998] relationship are only applicable for the epicentral distance less than 100 km and 150 km, respectively, which causes a larger difference beyond such distance when compared to the present study. It can be seen, from Figure 9(a-c), that the GMPEs for Himalayan region proposed by Bajaj and Anbazhagan [2019b] and Anbazhagan et al. [2013a] are significantly different from each other, which is attributed to the inclusion of the regional kappa factor by Bajaj and Anbazhagan [2019b]. Further, the PGA based on Raghukanth and Kavitha [2014] estimate the lesser PGA, for Mw = 4.0, 5.8 and 6.8, in comparison to the present study as well as the other study, since it used the amplification for the Indo-Gangetic region. However, the path attenuation was considered the same as that of the Himalayan region.

In this study, the source is modelled after considering the parameters of the Himalayan region however; the path is modelled according to the northern plains. This leads to the higher attenuation of the amplitude parameters which can be seen in Figure 9. NDMA [2010] relationship seems to predict closely to the present model beyond 120 km for $M_w \leq 6.8$. The higher kappa value of the Bihar region concerning the north Himalaya also leads to a reduction in amplitude. The PGA produced by GMPEs proposed by NDMA [2010], Anbazhagan et al. [2013a] and Bajaj and Anbazhagan [2019b] exhibits the same trend when compared with the new GMPE but differs due to attenuated peak in the Bihar region.

a)

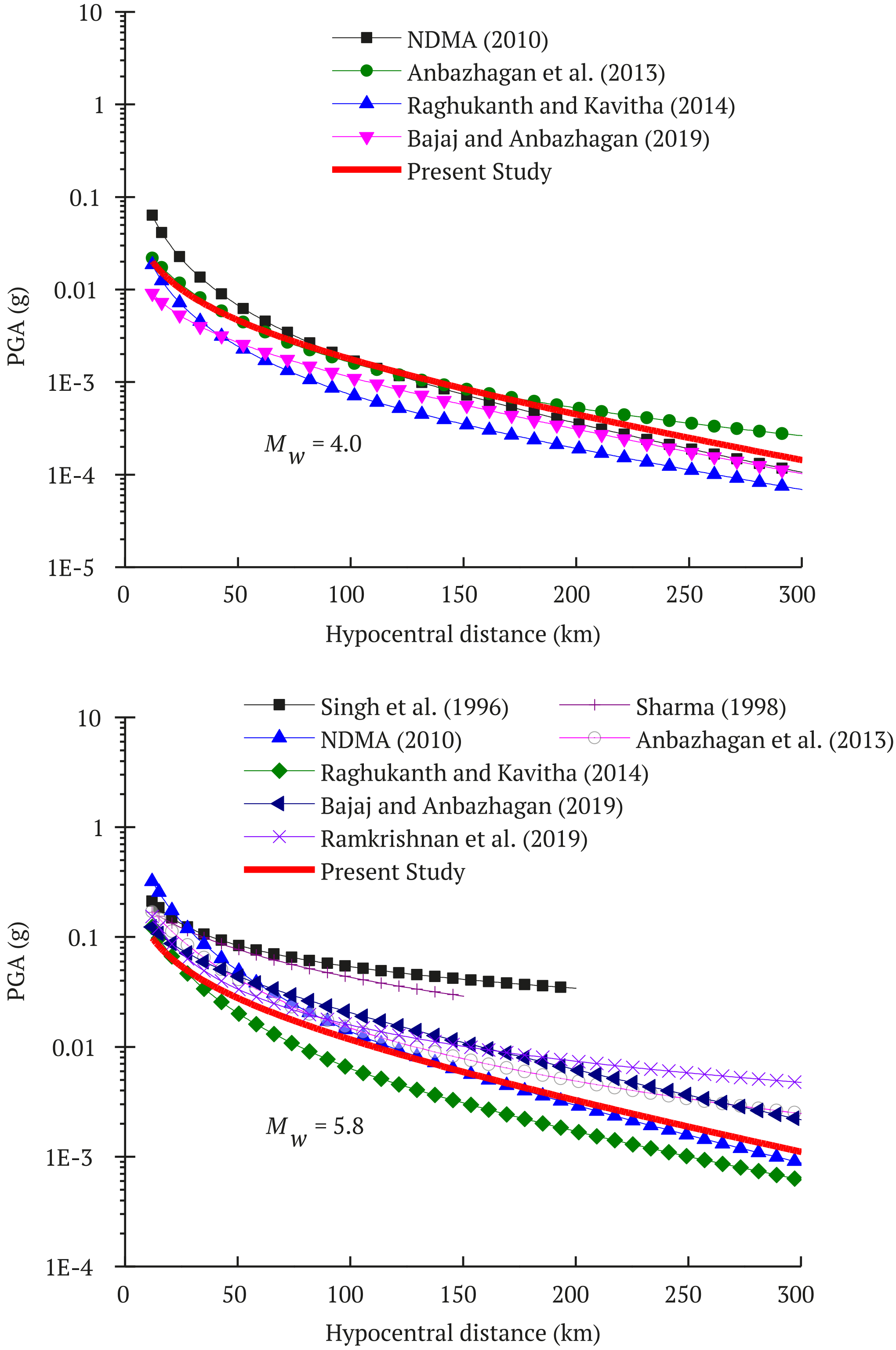

b)

Figure 9. Variation of PGA with distance using developed GMPE along with existing GMPEs for **(a)** for $M_w = 4.0$ **(b)** for $M_w = 5.8$ **(c)** for $M_w = 6.8$ **(d)** for $M_w = 8.5$.

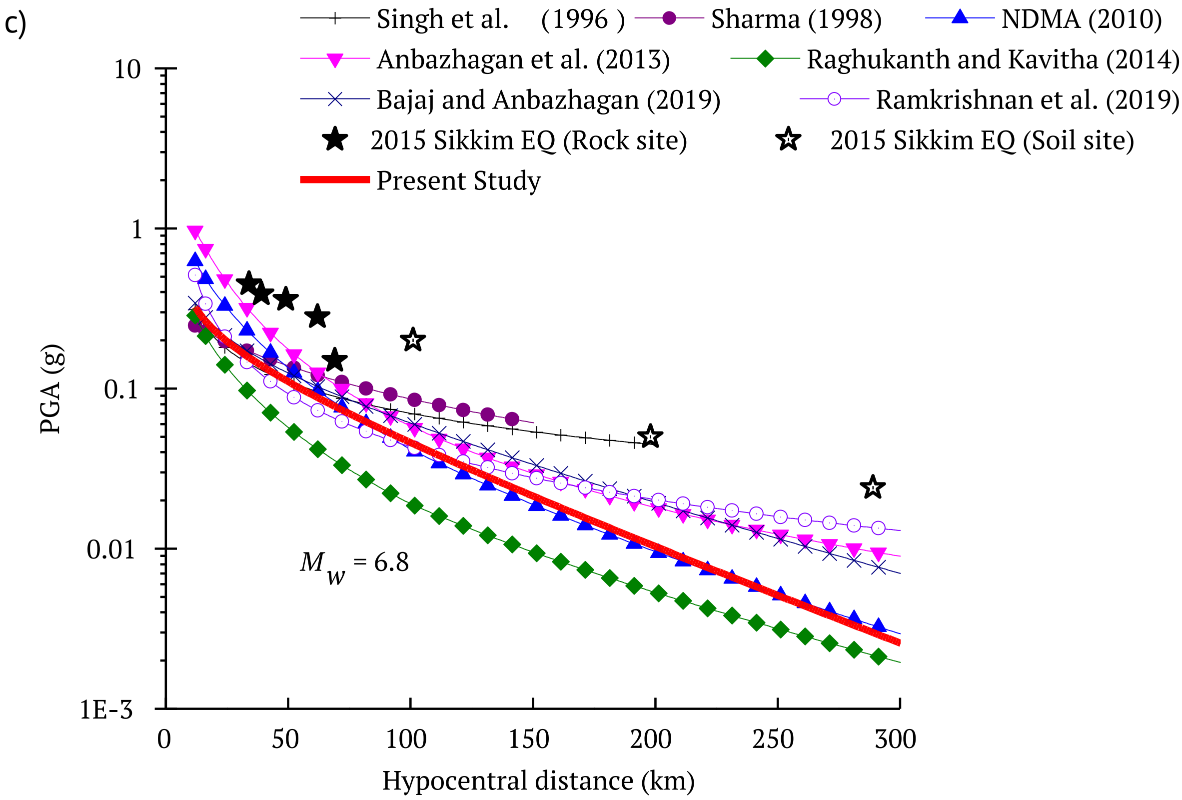
c)
Singh et al. (1996)
Sharma (1998)
NDMA (2010)
Anbazhagan et al. (2013)
Raghukanth and Kavitha (2014)
Bajaj and Anbazhagan (2019)
Ramkrishnan et al. (2019)
2015 Sikkim EQ (Rock site)
2015 Sikkim EQ (Soil site)
Present Study
PGA (g)
10
1
0.1
0.01
1E-3
M_w = 6.8
0
50
100
150
200
250
300
Hypocentral distance (km)

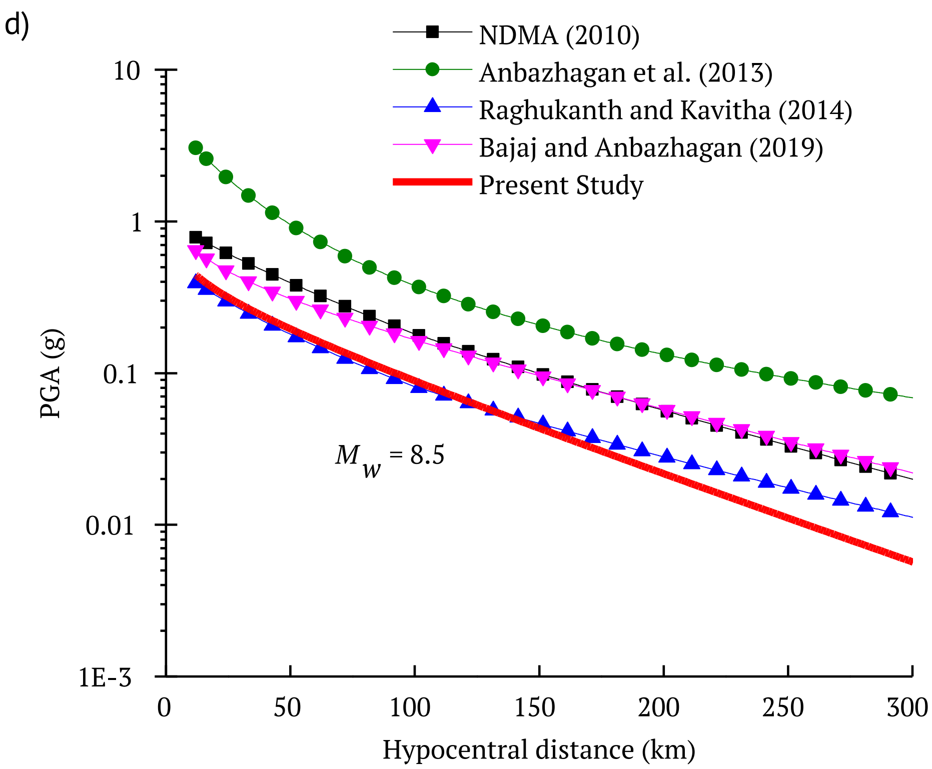
d)
NDMA (2010)
Anbazhagan et al. (2013)
Raghukanth and Kavitha (2014)
Bajaj and Anbazhagan (2019)
Present Study
PGA (g)
10
1
0.1
0.01
1E-3
M_w = 8.5
0
50
100
150
200
250
300
Hypocentral distance (km)

Figure 9.

5. Seismic Wave Amplification

The characteristics of soil deposits up to the depth of 30 m are very important in EQ engineering since amplification or de-amplification of ground motions are more prominent in this range [Nandy, 2007]. Many studies have employed various approaches to estimate ground motion amplification using seismological data and show its importance [Bajaj and Anbazhagan, 2019c; Harinarayan and Kumar, 2020b, Dammala et al., 2020]. The consideration of wave amplification becomes unavoidable due to the presence of overlain thick alluvial deposits causing large ground deformation which may result in large damage if amplification proceeds to a level where the seismic wave frequency becomes equal to the structure's resonance frequencies. The goal of most site response studies has been to identify areas with significant seismic danger due to ground motion amplification caused by surface geology. In the present study, an attempt is made to examine the seismic wave amplification and also the nature of amplification in the region.

5.1 Methodology to Assess Seismic Wave Amplification

1D Ground Response Analysis (GRA) is one of the interesting approaches to foresee the potential consequences of the EQ to identify the amplification of seismic waves. Though several approaches such as linear, equivalent linear as well as nonlinear are in practice to perform GRA, the equivalent linear approach has been utilised in this study. One dimensional equivalent linear seismic GRA considers the frequency domain analysis to estimate the response of soil deposits existing above the bedrock. In the equivalent linear GRA, the non-linear material models i.e., strain-dependent shear modulus and damping ratio of soil, are approximated as an equivalent linear material model using an iterative procedure. The iterative procedure incorporated in the DEEPSOIL (as shown in Figure 10) makes a compatible shear modulus and damping characteristics for an effective shear strain corresponding to the 65% maximum shear strain developed in each layer [Kramer, 1996]. In frequency domain analysis, the strain time histories obtained for each layer are used to identify the maximum strain which is further used in the estimation of effective shear strain. The computed effective shear strain for a given soil layer is then used to estimate the corresponding strain-compatible shear modulus and damping using iteration procedure. The iteration procedure is performed in equivalent linear analyses to ensure that the properties used in the analysis are compatible with the computed strain levels in all layers [Kramer, 1996]. This process is repeated until a convergent solution is obtained; for example, the number of steps mentioned in the Figure 10.

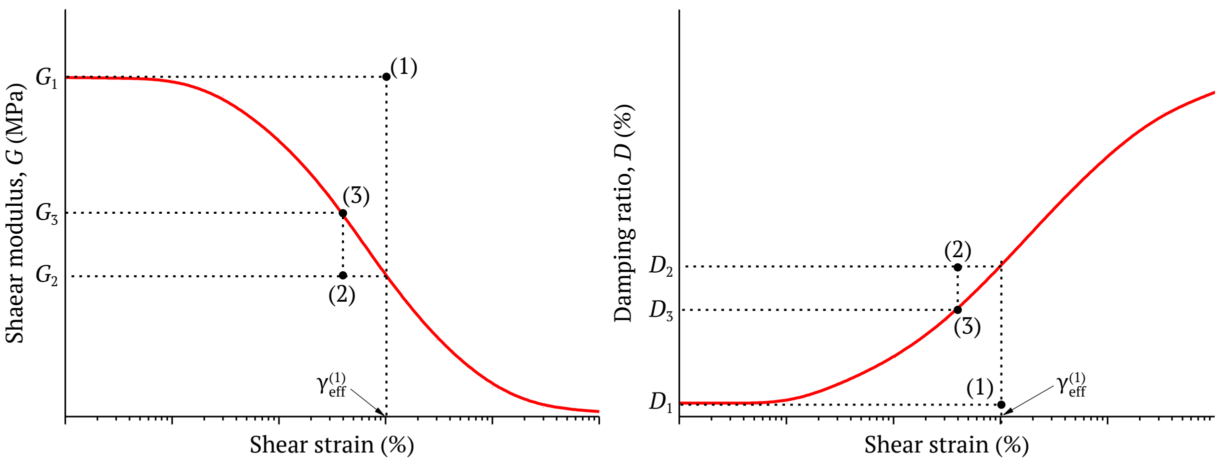

Figure 10. Iteration to make strain-compatible shear modulus and damping ratio in equivalent linear analysis [after Kramer, 1996].

Further, the equivalent linear GRA has been performed using DEEPSOIL [Hashash et al., 2018] with the assumptions that the layer of soil is horizontal and extended infinitely up to half space layer and, the seismic waves propagate vertically upward through a linear visco-elastic system from bedrock to soil deposits. The major input parameters required to perform GRA is the soil profile, at the site of interest, consisting of soil thickness, soil type, unit weight, shear wave velocity, material properties i.e., modulus reduction and damping ratio curve and, bedrock motion as an input motion. The simulated strong ground motions are used as an input motion in this study. Further, the shear wave velocity, which is an important parameter to characterise the soil stiffness, has been estimated using the widely used existing empirical correlations (mentioned in Table 6). It can also be stated that due to the unavailability of shear wave velocity profile at any particular site, the random selection of empirical correlation between *VS* and *SPT*-N might affect significantly the outcome of site-specific seismic GRA. It can also be noticed that the significant amount of uncertainty can be incorporated while using any one of the empirical correlations, from Table 6, therefore an averaging technique has been adopted to estimate an average empirical correlation of shear wave velocity for GRA as shown in Figure 11(b). From Figure 11b, it is seen that the average shear wave velocity profile is very close to the results obtained using Imai and Tonouchi [1982] and Uma Maheswari et al. [2008]. Uma Maheswari et al. [2008] have developed the empirical correlation for Indian soil. Finally, the empirical correlation based on the average shear wave velocity has been adopted for GRA and responses of the soil sites are plotted in Figure 11c.

S. No.	Author(s) Name	Correlations	Soil Type
1	Imai and Tonouchi [1982]	$v_s = 97\ N^{0.314}$	Applicable for all types of soils
2	Iyisan [1996]	$v_s = 51.5\ N^{0.516}$	
3	Kiku [2001]	$v_s = 68.3\ N^{0.292}$	
4	Hasancebi and Ulusay [2007]	$v_s = 90\ N^{0.309}$	
5	Uma Maheswari et al. [2008]	$v_s = 95.64\ N^{0.301}$	
6	Hanumantharao and Ramana [2008]	$v_s = 82.6\ N^{0.43}$	
7	Dikmen [2009]	$v_s = 58\ N^{0.39}$	

Table 6. Correlations for estimation of average $V_{s.}$

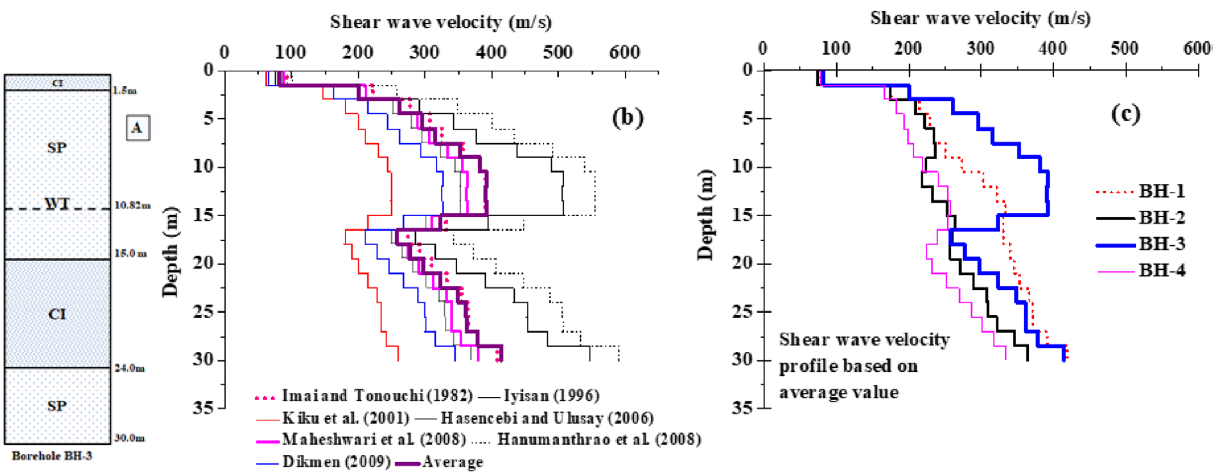

Figure 11. **(a)** Typical borehole profile (where, WT= water table, CI= Intermediate plastic clay, SP= poorly graded sand) **(b)** variations in shear wave velocity profile at BH-3 using all empirical correlations mentioned in Table 6 **(c)** variations in shear wave velocity profile at BH-1 to BH4 using empirical correlations based on average shear wave velocity.

5.2 Sub-soil Profile and Material Model

The entire Bihar region is covered by Alluvium soil consisting of loam soil, clay soil and silt soil up to the depth of bedrock level, which is significantly prone to the amplification or deamplifiaction of the seismic wave. Therefore, to see its potential evidence in the Bihar region, the sub-soil profile from four locations in Patna, Bihar, has been collected. Standard Penetration Tests (SPT) were performed in the Masaurhi area of Patna, Bihar, near NH-83 to characterise the soil conditions, at four locations namely BH-1, BH-2, BH-3 and BH-4, where BH indicates the Borehole and the numerals associated with BH indicates the number of borehole. It has been seen that all the Boreholes consisting clayey (low plastic) and sandy (poorly graded) soil with variations in water table up to 10 m from ground level. The plasticity index of soil was reported in the order of 5-30%. A typical borehole profile is presented in Figure 11a.

Further, the strain-dependent dynamic soil properties i.e., variation of shear modulus and damping ratio with shear strains are significantly important input parameters for the ground response analysis prior to the construction of any structures. Due to the unavailability of site-specific dynamic soil properties in the Bihar region, the modulus reduction and damping ratio curves existing in the DEEPSOIL were utilized in the analysis. In the present investigation, to characterize the dynamic feature of sands and clays, the standard curves for modulus reduction and damping ratio proposed by Seed and Idriss [1970] and Vucetic and Dobry [1991], shown in Figure 12, have been considered from the database of DEEPSOIL [Hashash et al., 2018]. The Plasticity Index (PI) values were chosen in the range of 5-30% for clay layers.

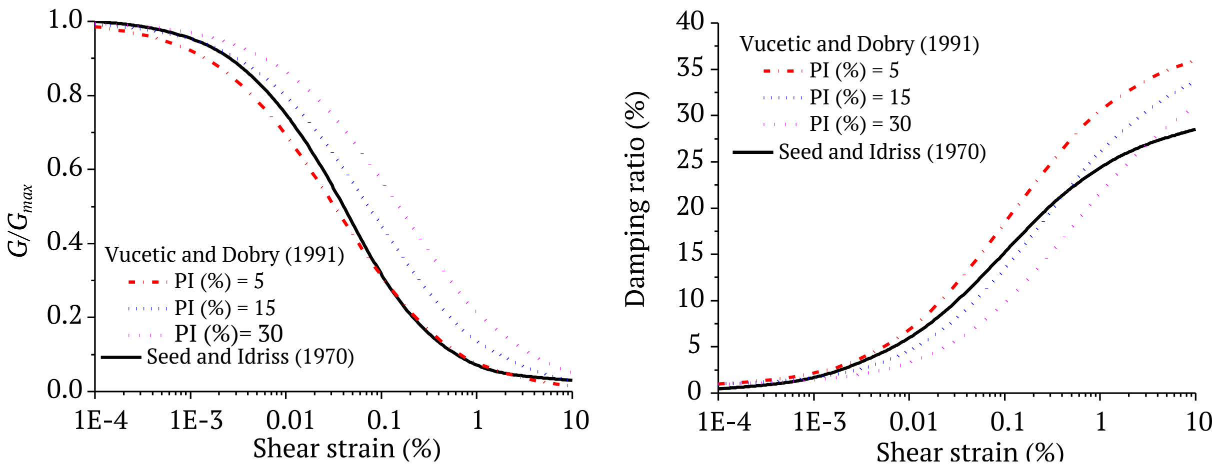

Figure 12. Material model used in 1D equivalent linear GRA (where, PI= Plasticity Index).

5.3 Strong Input Motion

Three synthetically generated acceleration time histories of PGA = 0.175g, 0.256g and 0.435g, corresponding to M_w7.8, M_w7.9 and M_w = 8.2, have been used for GRA; since Khattri [1999] has reported that the high probability of the occurrence of an EQ of $M_w > 8.0$, in near future, in the central seismic gap. Since the central seismic gap comes under seismic zone V [IS: 1893-2016], Nath et al. [2008a] have also reported that the average value of PGAs, for $M_w > 8$, can be 0.18 g, 0.23 g, 0.33 g, 0.50 g, and 0.82 g for low, moderate, moderately high, high and very high seismic hazards zones, respectively. As per IS: 1893 [2016], the seismic zone has been defined based on the consideration of effective peak ground acceleration, from the most severe earthquake (i.e., Maximum Credible Earthquake, MCE), and the service life of the structure in that region. IS: 1893 [2016] has also suggested that the design value of PGA = 0.36 g and 0.18 g considering Maximum Considered Earthquake (MCE) and Design Basis Earthquake (DBE, i.e., earthquake which is expected to occur at least once during the design life of the structure.) scenarios, respectively, should be adopted for the structural design. Thus, to observe the response of soil as well the effect of PGA during GRA, three different acceleration time histories of PGA ranging from PGA = 0.175g-0.435g, of the futuristic EQs in central seismic gap, has been chosen considering low, moderate, and high seismic hazards scenario of the study region.

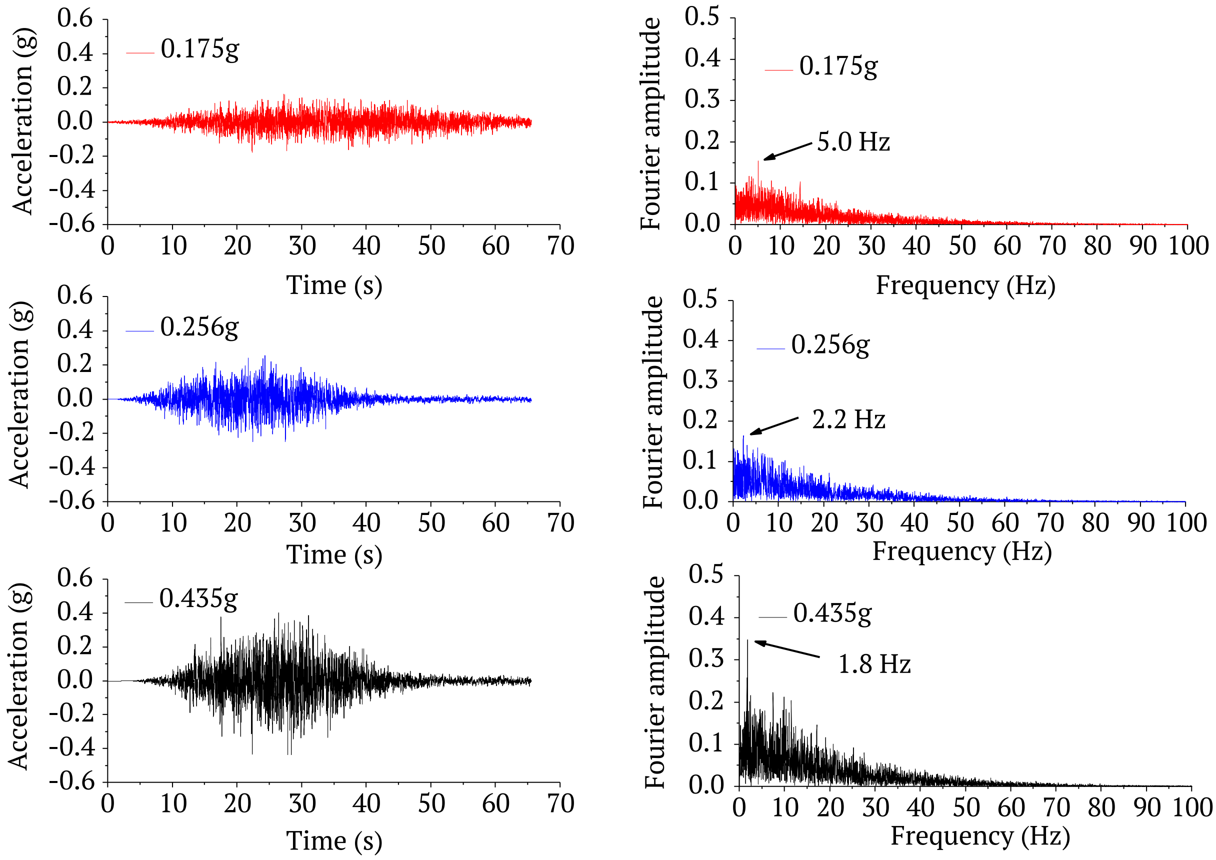

Figure 13. Acceleration time history of input motion and their Fourier amplitude.

Figure 13 presents the acceleration histories and their Fourier amplitude spectrum of input strong motions. Frequency-domain representation indicates the variation of energy content over a frequency band. It is observed that the maximum energy contents of strong motion are congregated over a fundamental frequency band of 1.0-5.0 Hz. The ground motion characteristics such as predominant period, mean period, bracketed duration and significant duration derived by using the SEISMOSIGNAL program (https://seismosoft.com) are shown in Table 7. The mean period of strong ground motions is varying from 0.27s to 0.31s, which represents the frequency content characterization parameter of the ground motions.

5.4 Assessment of Seismic Wave Amplification

Assessment of seismic wave amplification and other responses were carried out using one-dimensional seismic ground response analyses and, the results were reported in terms of the variations of maximum acceleration, maximum shear strain, maximum shear stress ratio and ground motion amplification along with depth. Figure 14 shows the variation of the aforementioned parameters for BH3. The variations in acceleration with depth, presented in Figure 14a, indicate that the acceleration at the ground surface is increased in comparison to the input acceleration. Figure 14b shows the variations in strain along with depth using input motion of PGA = 0.175g, 0.256g and 0.435g at BH3 and, it is seen that the shear strain was found to be maximum at the depth of 17.5m from the ground level due to presence of a relatively softer layer, indicated by SPT-N value. The variations of shear strain within the soil deposits not only depends on the confining depth and the energy of input motion, but also depending on the several other parameters associated with the strong motion such as arias intensity, specific energy density, predominant period, mean period, bracketed duration and significant duration [Kumar et al., 2018c].

Further, the maximum stress ratio was found to be in the range of 0.25 to 0.50, in Fig. 14c. Figure 14d presents the amplification and de-amplification of the seismic wave through the soil strata using input motion of PGA = 0.175g, 0.256g and 0.435g at BH3 and, it was found that the seismic wave gets amplified at ground level by 20% to 70% from

Parameters	Low	Moderate	High
Magnitude (M_w)	7.8	7.9	8.2
Station	Apparent station		
Site Class	A/B	A/B	A/B
Distance from source	65	60	65
Max. PGA (g)	0.175g	0.256g	0.435g
Predominant period (s)	0.12	0.08	0.14
Mean period (s)	0.278	0.312	0.279
Frequency (Hz)	3.6	3.2	3.6
Maximum velocity	21.62 cm/s at t=39.5s	32.45 cm/s at t=15.4s	46.32 cm/s at t=28.36s
Maximum displacement	60.27 cm at t=44.3s	46.88 cm at t=59.9s	69.29 cm at t=63.932s
Arias intensity (m/s)	1.31	1.94	4.96
Specific energy density (cm^2/s)	3702.58	4288.40	5152.13
Cumulative absolute velocity (cm/s)	1667.4	1719.87	2662.77
v_{max}/a_{max} (s)	0.124	0.128	0.109

Table 7. Strong motion parameters for simulated ground motion used in GRA.

the input motion PGA ranging from 0.175g-0.435g. Further, the analyses have been carried out for all boreholes i.e., for BH1 to BH4. Figure 15a shows the variations in acceleration with depth for BH1-BH4 and it can be seen that the acceleration at the ground surface is increased by 43% and 38% when analysed by input motion PGA = 0.175g and 0.435g, respectively. Figure 15b shows the variation in strain along with depth using input motion of PGA = 0.175g, 0.256g and 0.435g at BH1-BH4 and, it is seen that the strain was found to be maximum within the depth of 12.5m-20m when soil deposit encounter with high input PGA (= 0.435g) motion. Further, the maximum stress ratio was found to be in the range of 0.25 to 0.55, in Fig. 15c, for BH1-BH4. Figure 15d presents the amplification and de-amplification of the seismic wave through the soil strata at BH1-BH4 and, it was found that the seismic wave gets amplified at ground level by 10% to 70% from the input motion PGA ranging from 0.175g-0.435g. The amplification of seismic waves from bedrock to surface level is presented in terms of amplification factor in Table 8. It can be seen that the amplification factor at boreholes BH1-BH4 was in the range of 1.06 to 1.66 for input motion PGA ranging from 0.175g to 0.435g, which reflects that the seismic motion with lesser input bedrock PGA shows higher amplification in comparison to the seismic motion with higher input bedrock PGA. This is attributed to the fact that the high PGA values of input bed rock motion possess high value of shear strain into the soil deposit, due to high amount of soil nonlinearity, which causes high energy dissipation in a small time interval resulting in lesser amplification of seismic waves.

Input PGA	0.175g	0.256g	0.435g
AF of all boreholes	1.38-1.66	1.18-1.60	1.06-1.32

Table 8. Amplification of bedrock PGA.

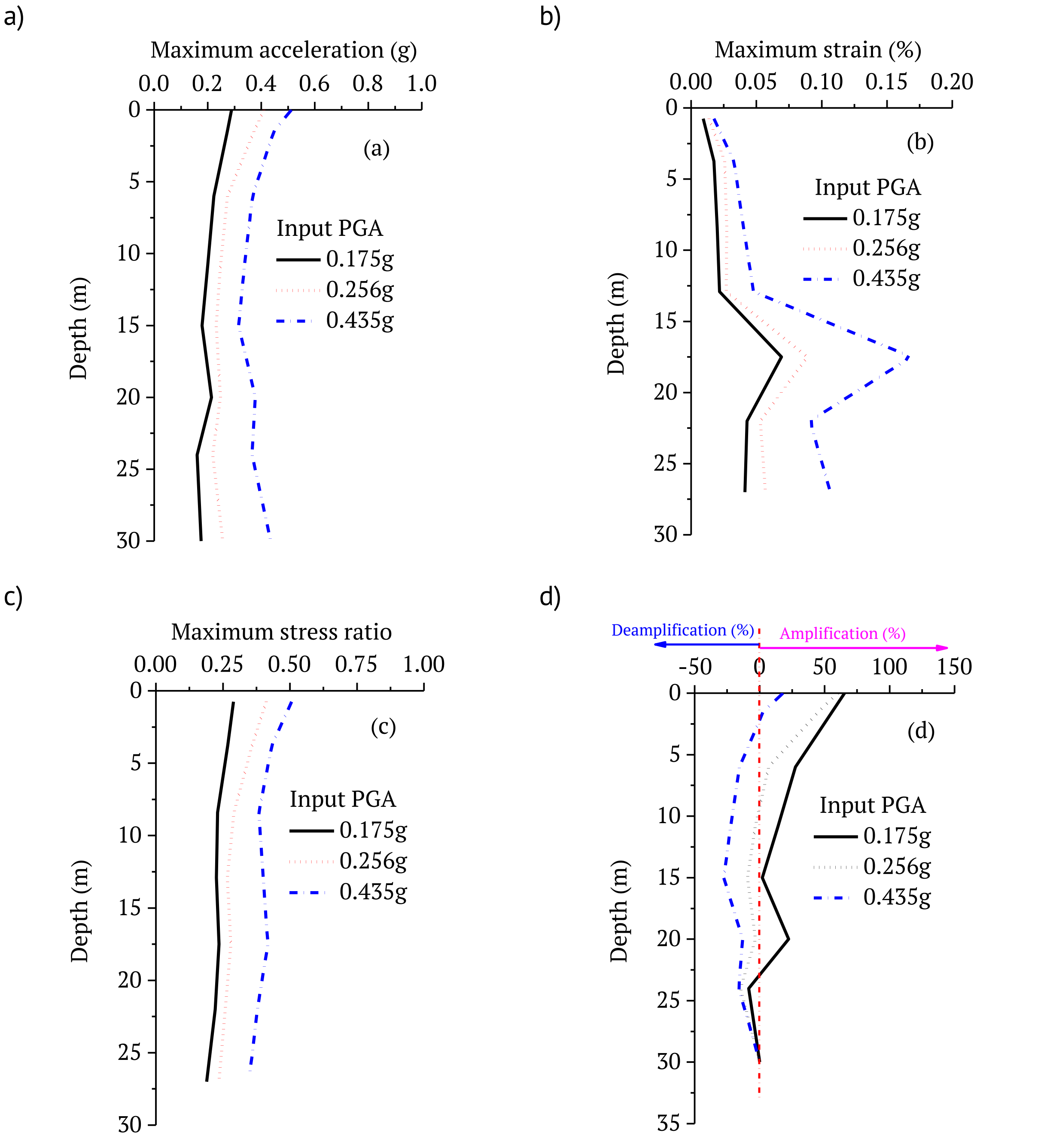

Figure 14. Variation of **(a)** maximum acceleration **(b)** maximum strain **(c)** maximum stress ratio and **(d)** amplification of seismic wave with depth at borehole BH-3 for different input excitations.

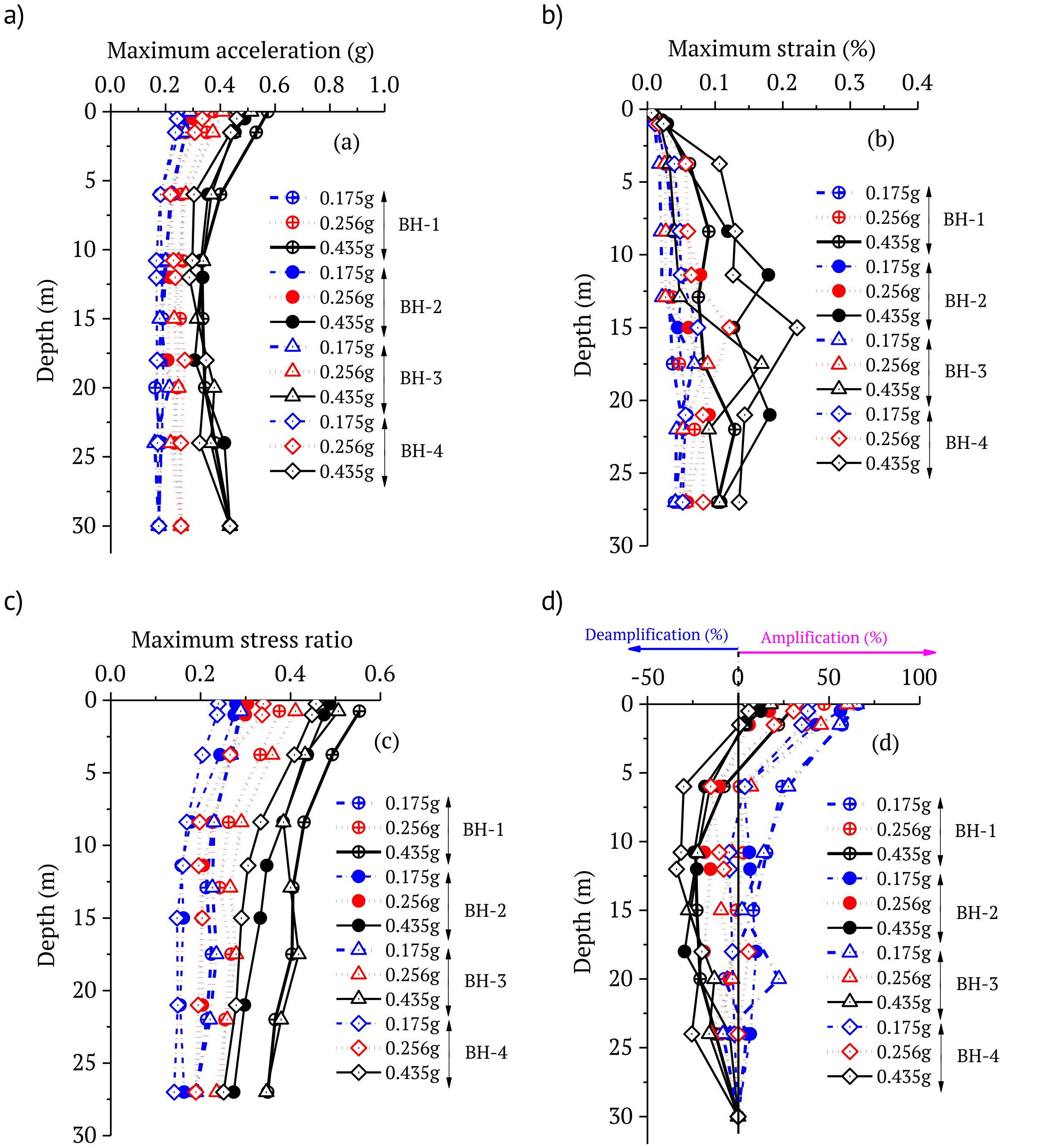

Figure 15. Variation of **(a)** maximum acceleration **(b)** maximum strain **(c)** maximum stress ratio and **(d)** amplification with depth for borehole BH1-BH4 for different input excitations.

5.5 Spectral Acceleration at Surface level

Strong ground motion and the associated seismic hazards are generally indicated by PGA. However, engineers always prefer to use the response spectrum as a better descriptor of seismic hazards, which is directly applicable to the design of structures [Kumar et al., 2018a]. The acceleration response spectrum at 5% damping ratio, describes the maximum response of a single degree of freedom system corresponding to a particular input motion and indicates the potential effects of an input motion on different structures.

Figures 16(a-d) present the variations of surface level spectral acceleration with periods, at four boreholes i.e., BH1-BH4, using synthetically generated bedrock input motion of PGA = 0.175g, 0.256g and 0.435g. The maximum spectral acceleration at surface level for BH1 was increased by approximately 60%, 56% and 27%, when bedrock input motion of PGA = 0.175g, 0.256g and 0.435g, respectively. Similar responses were observed for BH2, BH3 and BH4. It indicates that the input motion gets amplified or deamplified when it encounters the soil deposits, which is similar to the response of amplification of PGA at the surface level as shown in Fig. 15d. Figure 16(a-d) also indicates that the low and high amplitude of input motions (i.e., PGA = 0.175g, 0.256g and 0.435g) are responsible for the generation of low and high surface level spectral acceleration at the surface, respectively. From the results, it can be noticed that the soil deposit significantly affects the amplification/deamplification of seismic waves within the range of period 0.04 s-2.0 s, which is in the range of predominant frequency of EQs i.e., 0.5-10 Hz reported by Bhattacharya [2007]. Thus, from Figure 16(a-d), it can be stated that the characteristics of subsoil conditions as well as the amplification of seismic waves through existing subsoil are of utmost important to estimate the expected dynamic load coming on to the structures considering adequate factor of safety.

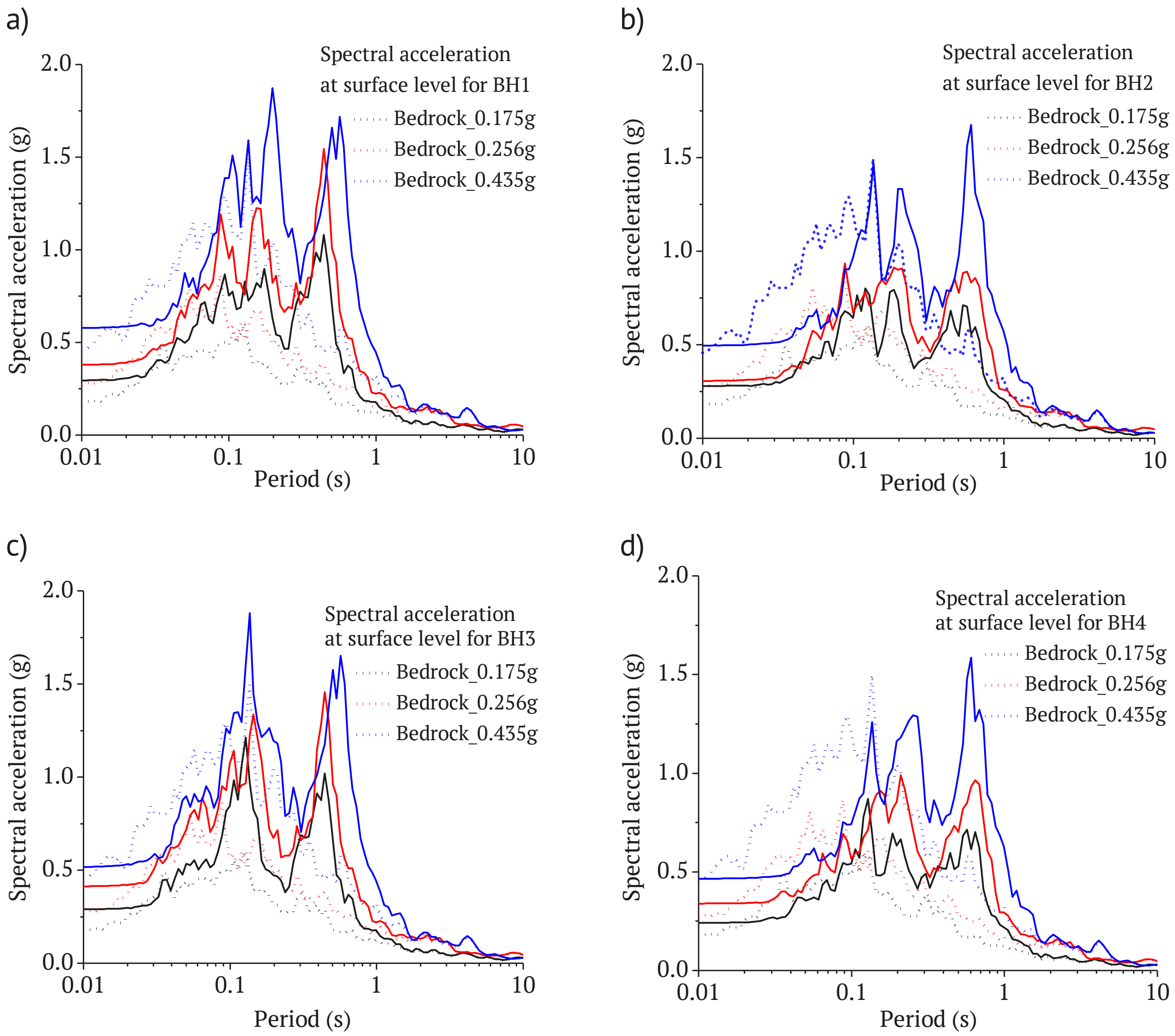

Figure 16. (a-d) Variations of spectral acceleration with period at surface level for BH1 to BH4 using bedrock motion of PGA = 0.175g, 0.256g and 0.435g.

6. Summary and Conclusions

A new region-specific GMPE has been developed for the Bihar region based on synthetically generated strong ground motion data, considering a moment magnitude range of 4.0 to 8.5, hypocentral distances till 300 km and convolution theorem. The stochastic method was considered with the incorporation of tri-linear variation of geometric attenuation and other region-specific seismological parameters to propose GMPE. Further, the Stochastic model was validated by checking the capability of the model to predict realistic EQs. Due to the lack of recorded ground motion for the Bihar region predicted result was compared with that of recordings from stations out of the study area, which opens the door for slight error in the predicted spectral acceleration values. The developed GMPE model has been compared with the existing GMPEs of the Indian region. However, validation of the model with recorded EQs at the stations in the Bihar region is desirable and may enhance the results in future. The least-square non-linear regression was performed for 500 datasets consisting of amplitude parameter, moment magnitude and hypocentral distance to obtain the predictive equation for spectral acceleration.

Moreover, the amplification of seismic waves was also analysed for four typical sites located at Patna considering three different synthetically generated ground motions of PGA = 0.175g, 0.256g and 0.435g reflecting low, moderate and high seismicity intensity of EQs. It was found that the acceleration at the ground surface increased by 43% and 38% when analysed by input motion PGA = 0.175g and 0.435g, respectively. It was also observed that the seismic wave gets amplified at ground level by 10% to 70% from the input motion PGA ranging from 0.175g-0.435g, indicating amplification and de-amplification of seismic wave presence of subsoils at BH1-BH4.

The maximum spectral acceleration at the surface level for BH1 was increased by approximately 60%, 56% and 27%, when bedrock input motion of PGA = 0.175g, 0.256g and 0.435g, respectively. Similar responses were observed for BH2, BH3 and BH4, which indicates that the low and high amplitude of input motions (i.e., PGA = 0.175g, 0.256g and 0.435g) are responsible for the generation of low and high spectral acceleration at surface level, respectively. Thus, from the aforementioned results and discussions, it can be suggested that the developed GMPE model for bed rock level, in this study, can be used to assess seismic hazards in the Bihar region.

References

Anbazhagan, P., C.V. Smitha, A. Kumar and D. Chandran (2013a). Estimation of design basis earthquake using region-specific M max, for the NPP site at Kalpakkam, Tamil Nadu, India, Nucl. Eng. Des., 259, 41-64.

Anbazhagan, P., A.Kumar and T.G. Sitharam (2013b). Ground motion prediction equation considering combined dataset of recorded and simulated ground motions, Soil Dyn. Earthq. Eng., 53, 92-108.

Anbazhagan, P., K. Bajaj and S. Patel (2015). Seismic hazard maps and spectrum for Patna considering region-specific seismotectonic parameters, Springer Netherlands, 1163-1195.

Atkinson, G.M. (2004). Empirical attenuation of ground-motion spectral amplitudes in southeastern Canada and the northeastern United States, Bull. Seismol. Soc. Am., 94, 1079-1095.

Atkinson, G.M. and D.M. Boore (1995). Ground-motion relations for eastern North America, Bull. Seismol. Soc. Am., 85, 17-30.

Atkinson, G.M. and D.M. Boore (2006). Earthquake ground-motion prediction equations for eastern North America, Bull. Seismol. Soc. Am., 96, 2181-2205.

Bajaj, K. and P. Anbazhagan (2018). Determination of GMPE functional form for an active region with limited strong motion data: application to the Himalayan region, J. Seismol., 22, 161-185.

Bajaj, K. and P. Anbazhagan (2019a). Comprehensive amplification estimation of the Indo Gangetic Basin deep soil sites in the seismically active area, Soil Dyn. Earthq. Eng., 127, 105855.

Bajaj, K. and P. Anbazhagan (2019b). Regional stochastic GMPE with available recorded data for active region-Application to the Himalayan region, Soil Dyn. Earthq. Eng., 126, 105825.

Bajaj, K. and P. Anbazhagan (2019c). Regional stochastic ground-motion model for low to moderate seismicity area with variable seismotectonic: application to Peninsular India, Bull. Earthq. Eng., 17, 3661-3680.

Banghar, A.R (1991). Mechanism Solution of Nepal-Bihar Eartbquake of August 20, 1988, J. Geol. Soc. India (Online Arch. from Vol. 1 to Vol. 78), 37, 25-30.

Baruah, S., S. Baruah, N.K. Gogoi, O. Erteleva, F. Aptikaev and J.R. Kayal (2009). Ground motion parameters of Shillong plateau: One of the most seismically active zones of northeastern India, Earthq. Sci., 22, 283-291.

Beresnev, I.A. and G.M. Atkinson (1998). FINSIM–a FORTRAN program for simulating stochastic acceleration time histories from finite faults, Seismol. Res. Lett., 69, 27-32.

Beresnev, I.A. and G.M. Atkinson (2002). Source parameters of earthquakes in eastern and western North America based on finite-fault modeling, Bull. Seismol. Soc. Am., 92, 695-710.

Bhatia, S.C., M.R. Kumar and H.K. Gupta (1999). A probabilistic seismic hazard map of India and adjoining regions, Ann. di Geofis., 42, 1153-1166.

Bilham, R. (2004). Earthquakes in India and the Himalaya: tectonics, geodesy and history, Ann. Geophys.

Bilham, R. (2015). Raising Kathmandu, Nat. Geosci., 8, 582-584.

Bird, J.F. and J.J. Bommer (2004). Earthquake losses due to ground failure, Eng. Geol., 75, 147-179.

Boore, D.M (1983). Stochastic Simulation o f High-frequency Ground Motions Based on Seismological Models of the Radiated Spectra, Bull. Seismol. Soc. Am., 73, 1865-1894.

Boore, D.M (2003a) Phase derivatives and simulation of strong ground motions, Bull. Seismol. Soc. Am., 93.

Boore, D.M (2003b) Simulation of ground motion using the stochastic method, Pure Appl. Geophys., 160, 635-676.

Boore, D.M. and G.M. Atkinson (1987). Stochastic prediction of ground motion and spectral response parameters at hard-rock sites in eastern North America, Bull. Seismol. Soc. Am., 77, 440-467.

Boore, D.M. and W.B. Joyner (1982). The empirical prediction of ground motion, Bull. Seismol. Soc. Am., 72, S43-S60.

Brune J.N (1970). Tectonic stress and the spectra of seismic shear waves from earthquakes, J Geophys Res, 75, 4997-5009.

Burnwal, M.L., A. Burman, P. Samui, and D. Maity (2017). Deterministic strong ground motion study for the Sitamarhi area near Bihar-Nepal region, Nat. Hazards, 87, 237-254.

Campbell, K.W. (1985). Strong motion attenuation relations: A ten-year perspective, Earthq. Spectra, 1, 759-804.

Campbell, K.W (1981). Near-source attenuation of peak horizontal acceleration, Bull. Seismol. Soc. Am., 71, 2039-2070.

Chandra, S. (1993). Fluvial landforms and sediments in the north-central Gangetic Plain, India., Darwin College, University of Cambridge, UK.

Choudhury, S.K. (1975). Gravity and Crustal Thickness in the Indo-Gangetic Plains and Himalayan Region, India, Geophys. J. R. Astron. Soc., 40, 441-452.

Dasgupta, S., M. Mukhopadhyay, and D.R. Nandy (1987). Active transverse features in the central portion of the Himalaya, Tectonophysics, 136, 255-264.

Dewey, J.F. and J.M. Bird (1970). Mountain belts and the new global tectonics, J. Geophys. Res., 75, 2625-2647.

Dikmen, Ü. (2009). Statistical correlations of shear wave velocity and penetration resistance for soils, J. Geophys. Eng., 6, 61-72.

Fukao, Y. and M. Obayashi (2015). Deep Earth Structure – Subduction zone structure in the mantle transition zone, edited by: Schubert, G. B. T.-T. on G. (Second E., Elsevier, Oxford, 641-654.

Fukushima, Y. and T. Tanaka (1990). A new attenuation relation for peak horizontal acceleration of strong earthquake ground motion in Japan, Bull. Seismol. Soc. Am., 80, 757-783.

Gansser, A.: Himalaya, Geol. Soc. London, Spec. Publ., 4, 267-278, 1974.

Geological Survey of India, Dasgupta, S., P.L. Narula, S.K. Acharyya and J. Banerjee (2000). Seismotectonic atlas of India and its environs, New Delhi.

Ghosh, T. and A. Mukhopadhyay (2013). Schematic Natural Hazard Zonation of Bihar using Geoinformatics, 2013.

Gupta, I.D. (2006). Delineation of probable seismic sources in India and neighbourhood by a comprehensive analysis of seismotectonic characteristics of the region, Soil Dyn. Earthq. Eng., 26, 766-790.

Gupta, I.D. (2010). Response spectral attenuation relations for in-slab earthquakes in Indo-Burmese subduction zone, Soil Dyn. Earthq. Eng., 30, 368-377.

Hanumantharao, C. and G.V. Ramana (2014). Dynamic soil properties for microzonation of Delhi, India, J. earth Syst. Sci., 117, 719-730.

Harbindu, A., S. Gupta and M.L. Sharma (2014). Earthquake ground motion predictive equations for Garhwal Himalaya, India, Soil Dyn. Earthq. Eng., 66, 135-148.

Harinarayan, N.H. and A. Kumar (2020). Determination of path attenuation and site characteristics of the north-west himalayan region and adjoining regions within the indian territory using generalized inversion method, Ann. Geophys., 63, 1-6.

Harinarayan, N.H. and A. Kumar (2020). Ground motion prediction equation for north India, applicable for different site classes, Soil Dyn. Earthq. Eng., 139.

Hartzell, S.H. (1978). Earthquake aftershocks as Green's functions, Geophys. Res. Lett., 5, 1-4.

Hasancebi, N. and R. Ulusay (2007). Empirical correlations between shear wave velocity and penetration resistance for ground shaking assessments, Bull. Eng. Geol. Environ., 66, 203-213.

Hashash, Y.M.A., M.I. Musgrove and J.A. Harmon (2018). Nonlinear and equivalent linear seismic site response of one-dimensional soil columns, User Man. v7. 0, Deep. Softw., 12.

Hayes, G.P. (2017). The finite, kinematic rupture properties of great-sized earthquakes since 1990, Earth Planet. Sci. Lett., 468, 94-100.

Https://seismosoft.com/products/seismosignal/; access on July 2022.

Imai, T. and K. Tonouchi (1982). Correlation of N-value with S-wave velocity: Proc. of 2nd Europ, Sympo. Penetration Test., 67-72.

IS 1893 Part-1 (2016).: Criteria for earthquake resistant design of structures, Bureau of Indian Satndard.

Iyengar, R.N. and S. Ghosh (2004). Microzonation of earthquake hazard in Greater Delhi area, Curr. Sci., 87, 1193-120.

Iyengar, R.N. and S.T.G. Raghu Kanth (2004). Seismological attenuation of strong ground motion in Peninsular India, Seismol. Res. Lett., 75, 530-540.

Iyisan, R. (1996). Correlations between shear wave velocity and in-situ penetration test results, in: Tech. J. Chamber Civil Eng. Turkey, 1187-99.

Jackson, J. (2002). Strength of the continental lithosphere: time to abandon the jelly sandwich, GSA Today, 12.

Jaiswal, A.K. and I.D. Gupta (2020). Probabilistic Seismic Hazard Mapping of Northwest India Using Area Sources with Non-Uniform Spatial Distribution of Seismicity, ISET Journal of Earthquake Technology, Paper No. 556, Vol. 57, No. 3, September 2020, pp. 103-150.

Joshi, D.D. and S.P. Bhartiya (1991). Geomorphic history and lithostratigraphy of a part of Eastern Gangetic plain, Uttar Pradesh, J. Geol. Soc. India (Online Arch. from Vol. 1 to Vol. 78), 37, 569-576.

Kanno, T., A. Narita, N. Morikawa, H. Fujiwara and Y. Fukushima (2006). A new attenuation relation for strong ground motion in Japan based on recorded data, Bull. Seismol. Soc. Am., 96, 879-897.

Kayal, J.R. (2008). Microearthquake seismology and seismotectonics of South Asia, Springer.

Khattri, K.N. (1987). Great earthquakes, seismicity gaps and potential for earthquake disaster along the Himalaya plate boundary, Tectonophysics, 138, 79-92.

Khattri, K.N. (1999). An evaluation of earthquakes hazard and risk in northern India, Himal. Geol., 20, 1-46.

Kijko, A. and G. Graham (1999). Parametric-historic" Procedure for probabilistic seismic hazard analysis part II: Assessment of seismic hazard at specified site, Pure Appl. Geophys., 154, 1-22.

Kiku, H. (2001). In-situ penetration tests and soil profiling in Adapazari, Turkey, in: Proc. 15th ICSMGE TC4 Satellite Conference on Lessons Learned from Recent Strong Earthquakes, August 25, 2001, Istanbul, Turkey, 259-265.

Kramer, S.L. (1996). Geotechnical Earthquake Engineering, Pearson Education India.

Kumar, A., N.H. Harinarayan and O. Baro (2017). Effects of earthquake motion and overburden thickness on strain behavior of clay and sany soils, 16th World Conf. Earthquake, 16WCEE, 1-13.

Kumar, A., N.H. Harinarayan, V. Verma, S. Anand, U. Borah and M. Bania (2018a). Seismic site classification and empirical correlation between standard penetration test n-value and shear wave velocity for Guwahati based on thorough subsoil investigation data, Pure Appl. Geophys., 175, 2721-2738.

Kumar, P., B.P. Chamoli, A. Kumar and A. Gairola (2019). Attenuation relationship for peak horizontal acceleration of strong ground motion of Uttarakhand region of central Himalayas, J. Earthq. Eng., 0, 1-18.

Kumar, S.S., A. Dey and A.M. Krishna (2018b). Importance of site-specific dynamic soil properties for seismic ground response studies: Ground Response Analysis, Int. J. Geotech. Earthq. Eng., 9, 78-98.

Kumar, S.S., A. Dey, and A.M. Krishna (2018c). Response of saturated cohesionless soil subjected to irregular seismic excitations. Natural Hazards, 93, 509-529.

Lermo, J. and F.J. Chávez-García (1993). Site Effect Evaluation using Spectral Ratios with only one Station, Bull. Seismol. Soc. Am., 83, 1574-1594.

Motazedian, D. and G.M. Atkinson (2005). Stochastic Finite-Fault Modeling Based on a Dynamic Corner Frequency, Bull. Seismol. Soc. Am., 95, 995-1010.

Mukhopadhyay, S. and J.R. Kayal (2003). Seismic tomography structure of the 1999 Chamoli earthquake source area in the Garhwal Himalaya, Bull. Seismol. Soc. Am., 93, 1854-1861.

Murphy, J.R.U. and L.J. O'brien (1977). The correlation of peak ground acceleration amplitude with seismic intensity and other physical parameters, Bull. Seismol. Soc. Am., 67, 877-915.

Nandy, D.R. (2007). Need for seismic microzonation of Kolkata megacity, in: Proceedings of workshop on microzonation, Indian Institute of science, Bangalore, India.

Nath, S.K., P. Sengupta and J.R. Kayal (2002). Determination of S-Wave Site Response in the Garhwal Himalaya from the Aftershock Sequence of the 1999 Chamoli Earthquake, Bull. Seismol. Soc. Am., 92, 1072-1081.

Nath, S.K., P. Sengupta, S.K. Srivastav, S.N. Bhattacharya, R.S. Dattatrayam, R. Prakash and H.V. Gupta (2003). Estimation of S-wave site response in and around Delhi region from weak motion data, Proc. Indian Acad. Sci. Earth Planet. Sci., 112, 441-462.

Nath, S.K., M. Vyas, I. Pal and P. Sengupta (2005). A seismic hazard scenario in the Sikkim Himalaya from seismotectonics, spectral amplification, source parameterization, and spectral attenuation laws using strong motion seismometry, J. Geophys. Res. Solid Earth, 110, 1-24.

Nath, S.K., K.K.S. Thingbaijam and A. Raj (2008a). Earthquake hazard in Northeast India - A seismic microzonation approach with typical case studies from Sikkim Himalaya and Guwahati city, J. Earth Syst. Sci., 117, 809-831, https://doi.org/10.1007/s12040-008-0070-6.

Nath, S.K., A. Raj, J. Sharma, K.K.S. Thingbaijam, A. Kumar, D.R. Nandy, M.K. Yadav, S. Dasgupta, K. Majumdar, J.R. Kayal, A.K. Shukla, S.K. Deb, J. Pathak, P.J. Hazarika, D.K. Paul and B.K. Bansal (2008b). Site amplification, Qs, and source parameterization in Guwahati region from seismic and geotechnical analysis, Seismol. Res. Lett., 79, 526-539.

Nath, S.K., A. Raj, K.K.S. Thingbaijam and A. Kumar (2009). Ground motion synthesis and seismic scenario in guwahati city-A stochastic approach, Seismol. Res. Lett., 80, 233-242.

Earthquake Catalogue: https://riseq.seismo.gov.in/riseq/Earthquake/archive, last access: 1 February 2023.

NDMA (2010). Development of probabilistic seismic hazard map of India, Technical Report of the Working Committee of Experts (WCE), National Disaster Management Authority (NDMA).

Ni, J. and M. Barazangi (1986). Seismotectonics of the Zagros continental collision zone and a comparison with the Himalayas, J. Geophys. Res. Solid Earth, 91, 8205-8218.

Parvez, I.A., F. Vaccari and G.F. Panza (2003). A deterministic seismic hazard map of India and adjacent areas, Geophys. J. Int., 155, 489-508.

Quittmeyer, R.C. and K.H. Jacob (1979). Historical and modern seismicity of Pakistan, Afghanistan, northwestern India, and southeastern Iran, Bull. Seismol. Soc. Am., 69, 773-823.

Raghu Kanth, S.T.G. and R.N. Iyengar (2007). Estimation of seismic spectral acceleration in Peninsular India, J. Earth Syst. Sci., 116, 199-214.

Raghukanth, S.T.G. (2008a). Ground motion estimation during the Kashmir earthquake of 8th October 2005, Nat. Hazards, 46, 1-13.

Raghukanth, S.T.G. (2008b). Simulation of strong ground motion during the 1950 Great Assam earthquake, Pure Appl. Geophys., 165, 1761-1787.

Raghukanth, S.T.G. and B. Kavitha (2014). Ground Motion Relations for Active Regions in India, Pure Appl. Geophys., 171, 2241-2275.

Ramkrishnan, R., K. Sreevalsa and T.G. Sitharam (2019). Development of New Ground Motion Prediction Equation for the North and Central Himalayas Using Recorded Strong Motion Data, J. Earthq. Eng., 0, 1-24.

Ramkrishnan, R., K. Sreevalsa and T.G. Sitharam (2020). Strong Motion Data Based Regional Ground Motion Prediction Equations for North East India Based on Non-Linear Regression Models, J. Earthq. Eng., 00, 1-21.

Scherbaum, F., F. Cotton and P. Smit (2004). On the use of response spectral-reference data for the selection and ranking of ground-motion models for seismic-hazard analysis in regions of moderate seismicity: The case of rock motion, Bull. Seismol. Soc. Am., 94, 2164-2185.

Seeber, L., J.G. Armbruster and K.H. Jacob (1999). Probabilistic assessment of seismic hazard for Maharashtra.

Seed, H.B. and I.M. Idriss (1970). Soil moduli and damping factors for dynamic response analysis, EERC.

Sreejaya, K.P., S.T.G. Raghukanth, I.D. Gupta, C.V.R. Murty and D. Srinagesh (2022). Seismic hazard map of India and neighbouring regions. Soil Dyn and Earthq Eng., 163, 107505.

Sharma, M.L. (1998). Attenuation relationship for estimation of peak ground horizontal acceleration using data from strong-motion arrays in India, Bull. Seismol. Soc. Am., 88, 1063-1069.

Sharma, M.L. and H. Bungum (2006). New strong ground-motion spectral acceleration relations for the Himalayan region, in: First European Conf Eearthq Eng and Seis., Vol. 1459.

Sharma, M.L., J. Douglas, H. Bungum and J. Kotadia (2009). Ground-motion prediction equations based on data from the himalayan and zagros regions, J. Earthq. Eng., 13, 1191-1210.

Singh, N.M., T. Rahman and I.G. Wong (2016). A new ground-motion prediction model for Northeastern India (NEI) crustal earthquakes, Bull. Seismol. Soc. Am., 106, 1282-1297.

Singh, R. and P.K. Khan (2021). Crustal Configuration and Seismic Stability of the Eastern Indian Shield and Adjoining Regions: Insights for Incidents of Great Earthquakes in the Nepal-Bihar-Sikkim Himalaya.

Singh, R.P., A. Aman and Y.J.J. Prasad (1996). Attenuation relations for strong seismic ground motion in the Himalayan region, Pure Appl. Geophys., 147, 161-180.

Singh, S.K., M. Ordaz, R.S. Dattatrayam and H.K. Gupta (1999). A spectral analysis of the 21 May 1997, Jabalpur, India, earthquake (Mw = 5.8) and estimation of ground motion from future earthquakes in the Indian shield region, Bull. Seismol. Soc. Am., 89, 1620-1630.

Sinha, R., P.F. Friend and V.R. Switsur (1996). Radiocarbon dating and sedimentation rates in the Holocene alluvial sediments of the northern Bihar plains, India, Geol. Mag., 133, 85-90.

Sinha, R., S.K. Tandon, P.S. Bhattarcharjee and A.S. Dasgupta (2005). Late Quaternary geology and alluvial stratigraphy of the Ganga basin, Himal. Geol., 26, 223-240.

Srivastava, H.N., M. Verma, B.K. Bansal and A.K. Sutar (2015). Discriminatory characteristics of seismic gaps in Himalaya, Geomatics, Nat. Hazards Risk, 6, 224-242.

Talebian, M. and J. Jackson (2004). A reappraisal of earthquake focal mechanisms and active shortening in the Zagros mountains of Iran, Geophys. J. Int., 156, 506-526.

Uma Maheswari, R., A. Boominathan and G.R. Dodagoudar (2008). Development of empirical correlation between shear wave velocity and standard penetration resistance in soils of Chennai city, in: Proc., 14th World Conf. on Earthq Eng., pp. 1-8.

Valdiya, K.S. (1976). Himalayan transverse faults and folds and their parallelism with subsurface structures of North Indian plains, Tectonophysics, 32, 353-386.

Verma, A.K., P. Pati and V. Sharma (2017). Soft sediment deformation associated with the East Patna Fault south of the Ganga River, northern India: Influence of the Himalayan tectonics on the southern Ganga plain. Journal of Asian Earth Sciences, 143, 109-121.

Vucetic, M. and R. Dobry (1991). Effect of soil plasticity on cyclic response, J. Geotech. Eng., 117, 89-107.

Wells, D.L. and K.J. Coppersmith (1994). New empirical relationships among magnitude, rupture length, rupture width, rupture area, and surface displacement, Bull. Seismol. Soc. Am., 84, 974-1002.

***CORRESPONDING AUTHOR: Shiv Shankar KUMAR**,

Department of Civil Engineering, National Institute of Technology (NIT) Patna-800005,

e-mail: k.shiv.ce@nitp.ac.in